

Calculation of the spin-polarized electronic structure of an interstitial iron impurity in silicon

H. Katayama-Yoshida* and Alex Zunger

Solar Energy Research Institute, Golden, Colorado 80401

(Received 8 November 1984)

We apply our self-consistent, all-electron, spin-polarized Green's-function method within an impurity-centered, dynamic basis set to study the interstitial iron impurity in silicon. We use two different formulations of the interelectron interactions: the local-spin-density (LSD) formalism and the self-interaction-corrected (SIC) local-spin-density (SIC-LSD) formalism. We find that the SIC-LSD approach is needed to obtain the correct high-spin ground state of Si:Fe⁺. We propose a quantitative explanation to the observed donor ionization energy and the high-spin ground states for Si:Fe⁺ within the SIC-LSD approach. For both Si:Fe⁰ and Si:Fe⁺, this approach leads to a hyperfine field, contact spin density, and ionization energy in better agreement with experiments than the simple LSD approach. The apparent dichotomy between the covalently delocalized nature of Si:Fe as suggested on the one hand by its reduced hyperfine field (relative to the free atom) and extended spin density and by the occurrence of two closely spaced, stable charge states (within 0.4 eV) and on the other hand by the atomically localized picture (suggested, for example, by the stability of a high-spin, ground-state configuration) is resolved. We find a large reduction in the hyperfine field and contact spin density due to the covalent hybridization between the impurity 3*d* orbitals and the tails of the delocalized *sp*³ hybrid orbitals of the surrounding silicon atoms. Using the calculated results, we discuss (i) the underlying mechanism for the stability and plurality of charged states, (ii) the covalent reduction in the hyperfine field, (iii) the remarkable constancy of the impurity Mössbauer isomer shift for different charged states, (iv) comparison with the multiple charged states in ionic crystals, and (v) some related speculation about the mechanism of (Fe²⁺/Fe³⁺) oxidation-reduction ionizations in heme proteins and electron-transporting biological systems.

I. EXPERIMENTAL CHARACTERISTICS OF Si:Fe

Iron is a low-solubility^{1,2} (1.5×10^{16} cm⁻³ at 1200°C), fast-diffusing³⁻⁵ ($D \sim 4 \times 10^{-6}$ cm²/sec at 1100°C) impurity in silicon, with a low distribution coefficient⁶ ($\sim 6 \times 10^{-6}$). It is present even in as-grown material² and is thought to have a controlling effect on thermally induced defects in quenched silicon.^{1,2} Even minute contamination by Fe ($\sim 10^{14}$ cm⁻³) are known⁷ to have a considerable effect ($\sim 50\%$) on the silicon solar cell's efficiency. Deep-level transient spectroscopy (DLTS) measurements have first identified an *E*(0/+) donor level (a Fe⁰→Fe⁺ transition) at $E_v + 0.45$ eV,⁸ or $E_v + 0.43$ eV,⁹ or $E_v + 0.46$ eV,¹⁰ where E_v is the valence-band maximum; however, when the temperature dependence of the (hole) capture cross section has been taken into account, the value turned out to be $E_v + 0.385 \pm 0.01$ eV. This was established by a combination of Hall effect and electron paramagnetic resonance (EPR) experiments¹¹ (yielding $E_v + 0.375$ eV), by a combination of DLTS and Hall effect¹² (yielding $E_v + 0.39 \pm 0.02$ eV), by a combination of DLTS and thermally stimulated capacitance (TSC) techniques¹³ ($E_v + 0.39$ eV), and directly from DLTS¹⁴ ($E_v + 0.383$ eV). These values are close to those determined from the temperature dependence of the Hall coefficient and resistivity⁶ and from the steep rise of the photoconductivity spectra.⁶ Attempts to identify acceptor states (a Fe⁰→Fe⁻ transition) of an isolated iron impurity

have failed.¹⁵ It can be concluded that this transition does not exist at least between the $E_v + 0.045$ eV to $E_c - 0.045$ eV (where E_c is the conduction-band minimum) and most likely does not exist at all in the band gap.¹⁵ Whereas a double donor *E*(+/2+) (a Fe⁺→Fe²⁺ transition) has been suggested as an explanation for the disappearance of the Fe⁺ EPR signal,¹⁶ it was not identified directly.¹⁵ EPR data^{1,2,11,15-18} for the neutral center show a distinct spectra due to interstitial Fe with a *g* factor of $g = 2.070$ and spin $S = 1$. The EPR parameters for the Fe centers in Si are summarized in Table I.¹⁸ Analysis of the data¹⁹ shows that the impurity hyperfine field (147.6 kG [Ref. 18(b)] or 152.2 kG [Ref. 18(a)]) and the spin density at the nucleus (0.282 a.u.⁻³ [Ref. 18(b)] or 0.299 a.u.⁻³ [Ref. 18(a)]) are considerably smaller than those characteristic of a free iron atom (calculated Hartree-Fock values²⁰ for *d*⁸, Fe⁰ give -350 kG for the hyperfine field and -0.668 a.u.⁻³ for contact spin density, respectively). This is also evident from recent electron-nuclear double-resonance (ENDOR) experiments,²¹ which show the spin density to be expanded at least up to the fifth Si shell and suggest that the localization of the spin density of Si:Fe⁰ could be estimated to be between 80% and 95%. The charged center Fe⁺ has a $S = \frac{3}{2}$ high-spin configuration^{18(a)} (S being the total electron spin) with a small hyperfine field (32.6 kG) and small spin density (0.0377 a.u.⁻³). We will be concerned here with isolated Fe impurities only. In addition to the data surveyed here for the isolated Fe impur-

TABLE I. Experimentally observed EPR parameter (Ref. 18), hyperfine coupling constant A (in units of 10^{-4} cm^{-1}), hyperfine field H_{hf} (in kG), effective electron spin density at the nucleus $|\phi(0)|_{\text{eff}}^2$, and spin density at the nucleus $\delta\rho(0)$ (both in units of a.u. $^{-3}$) for the Fe impurity in silicon (Ref. 19).

Configuration	Ion	S	J	g	g_N	A	$ \phi(0) _{\text{eff}}^2$	H_{hf}	$\delta\rho(0)$	Reference
$(3d)^7$	$(\text{Fe}^{57})^+$	$\frac{3}{2}$	$\frac{1}{2}$	3.524	+ 0.1804	2.99	0.0377	32.6	0.0377	18(a)
$(3d)^8$	$(\text{Fe}^{57})^0$	1	1	2.0699	+ 0.1804	6.98	0.1496	152.2	0.2992	18(a)
	$(\text{Fe}^{57})^0$	1	1	2.0700	+ 0.1804	6.57	0.1408	147.6	0.2816	18(b)

ity in silicon, there are abundant data on Fe-acceptor complexes, iron precipitates, and radiation-induced iron defects (surveyed in Refs. 5 and 16) that will not concern us here. The distribution of the superhyperfine interactions among the various ligand neighboring shells,²¹ the isotropy of the g tensor and the hyperfine interactions,^{16,17} and the appearance of two well-resolved fine-structure lines under uniaxial stress¹⁷ suggest that isolated iron takes up an undistorted tetrahedral interstitial site in silicon. The location of iron in the open interstitial site is also consistent with its ultrafast diffusivity in silicon.⁵ Whereas no static Jahn-Teller (JT) distortions were observed,^{16,17,21} a dynamic distortion cannot be ruled out.²² Only a small ($\sim 3\%$) outward breathing mode relaxation of the first shell of neighbors is expected.²³ Early Fe^{57} Mössbauer isomer-shift (IS) measurements^{24(a)} show for Si:Fe^0 that the isomer shift (Δ_{IS}) is 0.505 mm/sec. Since the IS (proportional to the negative of the charge density at the nucleus) increases as the number of s electron decreases, this result [intermediate between the result $\Delta_{\text{IS}}=0.15$ mm/sec for metallic iron²⁵ ($\sim d^7s^1$) and its dihalides²⁵ (d^6s^0) ($\Delta_{\text{IS}}=1.4$ mm/sec, d^6s^0)], suggests that Si:Fe^0 has an effective s -electron occupation between 0 and 1. More spectacularly, no change in the IS was found^{24(a)} in going from Si:Fe^0 to Si:Fe^+ , whereas such ionizations for iron in ionic crystals [e.g. (see Ref. 25) FeF_2 versus FeF_3] show huge changes ($1.4-0.46=0.94$ mm/sec). However, the Mössbauer data available to date on Si:Fe are clouded by the occurrence of complexes.^{24(b)} We will indicate the clear-cut prediction of theory on this matter.

II. DUALITY OF Si:Fe WITH RESPECT TO LOCALIZATION

The experimental data on Si:Fe paradoxically suggest both a model of a covalently delocalized impurity and its opposite: that of an atomically localized impurity. Arguing for the former, we note the following. First, the impurity hyperfine field H_{hf} and the contact spin density^{18(a),18(b)} $\delta\rho(0)$ at the nucleus of Si:Fe^0 are reduced by 43% relative to the free-atom value (using the calculated Hartree-Fock value²⁰ of Fe^0 , d^8), whereas these quantities for Fe in ionic solids²⁶ are close to the free-ion values. A similar conclusion is apparent from a recent electron-nuclear double-resonance experiment,²¹ which shows the spin density to be expanded at least up to the fifth Si shell surrounding the impurity. Second, as noted by Ludwig and Woodbury,^{18(a)} the EPR parameters, including the spin values for neutral Si:Fe^0 ($S=1$) and the charged ion

Si:Fe^+ ($S=\frac{3}{2}$) indicate that the s electrons of the free atom (d^6s^2) are converted in the solid into d orbitals (d^8 for Fe^0 , d^7 for Fe^+). However, this $s \rightarrow d$ population inversion must suggest a substantial delocalization: If the impurity orbitals were atomically localized, the strong s - d Coulomb repulsion energy U^{sd} would have resisted such a transfer. (In free atoms,²⁷ even the d^7s^1 configuration is about 5 eV above the d^6s^2 ground state. $3d$ impurities in ionic crystals²⁸ similarly show a $s \rightarrow d$ excitation energy of 5–6 eV). Third, the stability of the “overcrowded” d^8 configuration also suggests substantial delocalization. The $(\text{Fe}^0/\text{Fe}^+)$ donor ionization energy^{5,9,11–13} $E(0^+)=E_v+0.385\pm 0.01$ eV, when referred to vacuum [i.e., subtracting it from the position of the valence-band maximum E_v relative to vacuum, approximately 5.2 ± 0.2 eV (Ref. 29)] is $\sim 4.8\pm 0.2$ eV. This value is characteristic of the far stabler doubly ionized Fe^{2+} system [e.g., the $(\text{Fe}^{2+}/\text{Fe}^{3+})$ ionization in GaP, GaAs, and InP is^{30,31} 5.0 ± 0.05 eV]. In a polar electrolyte solution, the $(\text{Fe}^{2+}/\text{Fe}^{3+})$ redox potential³² is close to this, being around 5.0–5.3 eV. If the d electrons were atomically localized on the Fe impurity, the $(\text{Fe}^0/\text{Fe}^+)$ ionization energy would have been reduced relative to the $(\text{Fe}^{2+}/\text{Fe}^{3+})$ ionization energy (30.6 eV in the free ion²⁷) by twice the atomic d - d Coulomb repulsion energy U^{dd} (about 15–25 eV for $3d$ ions²⁷); hence, Fe^0 , d^8 would have been unbound.

These observations suggest a picture of a substantial expansion of the impurity d orbitals, perhaps through covalent hybridization, with the attendant reduction in the U^{sd} and U^{dd} Coulomb repulsion energies, a partial delocalization of the spin density, and a reduced exchange splitting Δ_x . It is also consistent with the anticipated^{33(a)} large crystal-field splitting Δ_{CF} (which increases with covalency and is³⁰ already 0.45 eV in the less covalent GaP:Fe system). We refer to this picture as the “covalently delocalized model” (CDM).

This CDM would have been complete, were it not for substantial evidence from the same experimental data that suggests the opposite conclusion, i.e., that of an “atomically localized model” (ALM). First, Si:Fe^+ appears similar to the free ion in a (Hund’s rule) high-spin ($S=\frac{3}{2}$) configuration,¹⁸ indicating that as large as the crystal-field splitting Δ_{CF} may be, the impurity orbitals must be sufficiently localized to have an exchange splitting Δ_x that exceeds Δ_{CF} . Second, despite the propagation of the spin density up to at least five shells of Si ligands, as much as 80–95% of the spin density is localized in the impurity central cell.²¹ Third, the electron-phonon cou-

pling of the impurity to the host crystal must be sufficiently weak (Δ_x is large) to explain the absence¹⁸ of any measurably static JT distortion in Si:Fe⁺ despite the degeneracy of its ⁴T₁ ground state. Fourth, the total angular momentum J is consistent with the interpretation¹⁸ of atomically localized $3d$ electrons. Fifth, the very low solubility and superfast diffusivity⁵ suggest a weak interference with the solid, i.e., that no strong bonds are formed or broken upon insertion or migration of Fe in silicon. Finally, although the Si band gap is too small for readily observing the atomlike $d \rightarrow d^*$ multiplet excitations (they are expected to occur in the infrared region), such transitions, characteristic of localized states³⁰ are observed for Fe impurities in wider gap semiconductors [e.g., (see Ref. 30), GaAs, InP, GaP] and are also likely to be found in silicon.^{33(a)}

The purpose of this paper is (i) to resolve the paradoxical duality in the nature of the localization in Si:Fe, (ii) to provide a physical understanding of the reduction in the hyperfine field and the ionization energy relative to the free atom, (iii) to give an explanation of the extended spin density observed by ENDOR, and (iv) to give a quantitative theory to the hyperfine field and the donor ionization energy.

III. METHOD OF CALCULATION

A. General theory

We apply the impurity Green's-function method developed by us previously,^{34,35} with the following modifications needed for the current applications: (i) since we are now interested in nuclear contact spin densities, which are dominated by core-polarization effects, we cannot use a coreless (pseudopotential) model³⁵ for the impurity atom. Instead, we use an all-electron impurity representation, where both the core and the valence orbitals are treated as spin-polarizable states on the same footing. (ii) The great sensitivity of core polarization to basis set effects suggests to us that a nonlinearly varied basis would be far more effective than a linearly varied set. Hence, we optimize the impurity-centered $1s$, $2s$, $2p$, $3s$, $3p$, $3d$, $4s$, $4p$, $4d$, and $4f$ spin-polarized dynamic basis orbitals at each self-consistency iteration by numerically integrating the atomlike Schrödinger equation of Fe within the impurity orbital subspace. As this dynamical basis set is updated iteratively, responding to changes in the self-consistent potential, we economize on the basis size using only the $1s$ through $4f$ orbitals. (iii) We have experimented with the Williams *et al.*³⁶ method to generate a variationally flexible Green's function, instead of the equivalent quasiband approach.³⁵ We find these methods to work equally well for Si:Fe, for which both methods were applied. (We continue to use the quasiband approach in pseudopotential calculations, and the Williams *et al.* approach for all-electron calculations.)

Since the perturbation potential due to a deep impurity is usually localized near the impurity site, the space spanned by the basis set can be divided into two subspaces. Subspace I with wave function $\psi^{(I)}(\mathbf{r})$ overlaps the perturbation potential of the impurity, whereas subspace

II with wave function $\psi^{(II)}(\mathbf{r})$ is orthogonal to subspace I and is affected little by the perturbation potential. The impurity wave functions, $\psi_{\text{imp}}(\mathbf{r})$, can be written as

$$\psi_{\text{imp}}(\mathbf{r}) = \psi^{(I)}(\mathbf{r}) + \psi^{(II)}(\mathbf{r}), \quad (1)$$

where $\langle \psi^{(I)}(\mathbf{r}) | \psi^{(II)}(\mathbf{r}) \rangle = 0$. Since in the impurity Green's-function approach it is sufficient to use basis functions where the perturbation potential is nonzero, all further calculations will be limited to subspace I (hereafter referred to as the impurity orbital subspace).

B. Host crystal bands

The Bloch functions $\phi_n(\mathbf{k}, \mathbf{r})$ of the host (H) silicon crystal are expanded in an LCAO (linear combination of atomic orbitals) form using ten (s , p , d , and f) Slater orbitals³⁷ $F_l^{(H)}(|\mathbf{r}|)$, i.e., $re^{-\alpha_1 r}$, $xre^{-\alpha_2 r}$, $yre^{-\alpha_2 r}$, $zre^{-\alpha_2 r}$, $(x^2 - y^2)e^{-\alpha_2 r}$, $(3z^2 - r^2)e^{-\alpha_2 r}$, $xye^{-\alpha_2 r}$, $yze^{-\alpha_2 r}$, $zxe^{-\alpha_2 r}$, and $xyze^{-\alpha_1 r}$ centered on each silicon site. The Bloch functions $\phi_n(\mathbf{k}, \mathbf{r})$ are given by the Fourier transformation of $F_l^{(H)}(\mathbf{r} - \mathbf{R}_i)$, where n denotes the band index (a combination of the angular momentum l and the partner index λ) and \mathbf{R}_i is the lattice site vector. These ten Slater orbitals centered on each silicon site are sufficient to reproduce the empirically fitted pseudopotential band structure.³⁸ The exponents α_1 and α_2 are $1.9(2\pi/a)$ and $2.0(2\pi/a)$, respectively, where a is the lattice constant of silicon. To evaluate the Hamiltonian matrix conveniently, we expand these $\phi_n(\mathbf{k}, \mathbf{r})$ in a plane-wave basis as before,³⁵ using about 80 plane waves (kinetic energies lower than 80 eV). Since it is not possible to reproduce with any useful accuracy the experimentally observed interband transitions by an *ab initio* pseudopotential using the local-spin-density formalism, we adjust the pseudopotential to reproduce the overall results of Cohen and Bergstresser.³⁸ Figure 1 depicts the LCAO band structure along with its

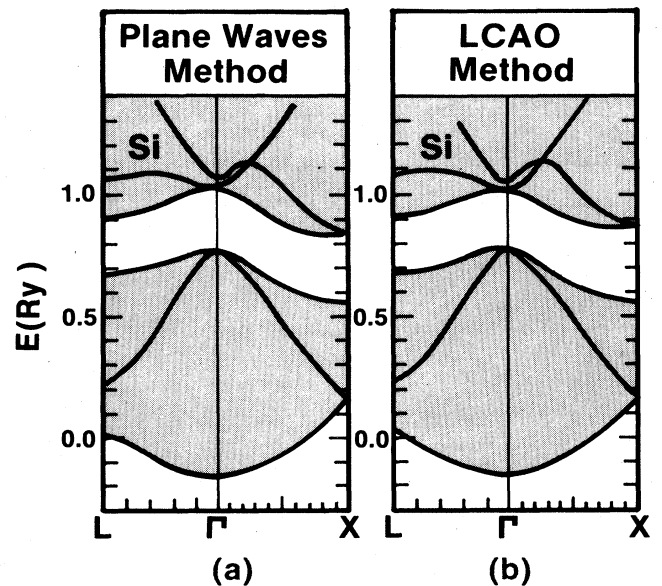


FIG. 1. Calculated band structure for silicon by (a) the plane-waves method and (b) the LCAO method, both using the same crystal pseudopotential.

parent plane-wave band structure. The two are in good agreement with each other (e.g., the band gap and the width of the valence band are 1.09 and 12.4 eV in the LCAO basis and are 1.07 and 12.7 eV in the plane-wave basis).

C. Basis functions in the impurity orbital subspace

The basis set spanning the impurity orbital subspace consists of local host basis functions and local impurity basis functions. Both are impurity centered.

1. Impurity-centered host basis set

For the local host basis set we choose the same radial orbitals $F_l^{(H)}(|\mathbf{r}|)$ that were used in the host crystal LCAO band structure in Sec. III B, however, we translate them to be impurity centered,³⁵ i.e.,

$$f_l^{\Gamma,\lambda}(\mathbf{r}) = F_l^{(H)}(|\mathbf{r}|) K_l^{\Gamma,\lambda}(\hat{\mathbf{r}}), \quad (2)$$

where $F_l^{(H)}(|\mathbf{r}|)$ denotes hostlike radial basis functions for angular momentum $l=s, p, d, \text{ and } f$, centered on the impurity site, and $K_l^{\Gamma,\lambda}(\hat{\mathbf{r}})$ are the Kubie harmonics with the same origin. Here, Γ denotes the representation, and λ is the partner index. Using this impurity-centered local host orbital $f_l^{\Gamma,\lambda}(\mathbf{r})$, we calculate the ordinary unperturbed Green's function $G_{l\lambda,l'\lambda'}^{0,\Gamma}(\epsilon)$ projected on the $f_l^{\Gamma,\lambda}(\mathbf{r})$ orbital at the tetrahedral interstitial impurity site as

$$G_{l\lambda,l'\lambda'}^{0,\Gamma}(\epsilon) = \sum_{n,\mathbf{k}} \frac{\langle \Gamma, l, \lambda | n, \mathbf{k} \rangle \langle n, \mathbf{k} | \Gamma, l', \lambda' \rangle}{\epsilon - \epsilon_{n,\mathbf{k}}}, \quad (3)$$

where $|\Gamma, l, \lambda\rangle$ compactly denotes $f_l^{\Gamma,\lambda}(\mathbf{r})$, whereas $|n, \mathbf{k}\rangle$ denotes the Bloch states $\phi_n(\mathbf{k}, \mathbf{r})$ for band index n and wave vector \mathbf{k} , and $\epsilon_{n,\mathbf{k}}$ are the corresponding band-structure energies.

2. Impurity basis set

In addition to the hostlike basis functions $f_l^{\Gamma,\lambda}(\mathbf{r})$, we define also the impurity (I)-like basis function $g_{\mu l \sigma}^{\Gamma,\lambda}(\mathbf{r})$ in analogy with Eq. (2), as³⁵

$$g_{\mu l \sigma}^{\Gamma,\lambda}(\mathbf{r}) = F_{\mu l \sigma}^{(I)}(|\mathbf{r}|) K_l^{\Gamma,\lambda}(\hat{\mathbf{r}}). \quad (4)$$

Here, $F_{\mu l \sigma}^{(I)}(|\mathbf{r}|)$ are the spin-dependent numerical impurity (I) radial orbitals with the principle quantum number μ , orbital momentum l , and spin index $\sigma = +$ for majority-spin states, and $\sigma = -$ for minority-spin states. We extend μl to $1s, 2s, 2p, 3s, 3p, 3d, 4s, 4p, 4d, \text{ and } 4f$.

Since core polarization is very sensitive to the basis set,²⁰ we choose a nonlinearly varied ("dynamic") impurity basis set. We optimize the impurity-centered local-impurity orbitals $g_{\mu l \sigma}^{\Gamma,\lambda}(\mathbf{r})$ iteratively by solving the "effective impurity Schrödinger equation," given by

$$\left[-\frac{1}{2}\nabla^2 + \Delta V^\sigma(|\mathbf{r}|) + V^{(H)}(|\mathbf{r}|) \right] F_{\mu l \sigma}^{(I)}(|\mathbf{r}|) = \epsilon_{\mu l \sigma} F_{\mu l \sigma}^{(I)}(|\mathbf{r}|). \quad (5)$$

Here, $\Delta V^\sigma(|\mathbf{r}|)$ denotes the perturbation potential determined from the Green's-function problem (see below), and $V^{(H)}(|\mathbf{r}|)$ is the fixed host crystal potential at the interstitial region evaluated as in Ref. 39. Since the spin and charge densities extend beyond the impurity site itself, we use a single site but extended basis sets³⁵ $\{g_{\mu l \sigma}^{\Gamma,\lambda}(\mathbf{r})\}$ and $\{f_l^{\Gamma,\lambda}(\mathbf{r})\}$, spanning a large volume around the impurity. During the self-consistency iterations, not only the linear coefficients of $\{g_{\mu l \sigma}^{\Gamma,\lambda}(\mathbf{r})\}$ are modified, but so is the poten-

tial of Eq. (5). As a result, changes in the wave function amplitude both at the impurity nucleus and its neighbors are taken into account in the self-consistency cycle. Note, however, that only the *impurity-induced changes* in charge and spin densities need to be updated iteratively in this Green's-function approach.

The impurity orbital subspace can be decomposed in the case of an interstitial $3d$ impurity into the irreducible representations of the T_d group as $a_1, t_2, \text{ and } e$. The a_1 representation is formed from the $1s, 2s, 3s, 4s, \text{ and } 4f$ orbitals; the t_2 representation is formed from the $2p, 3p, 3d, 4d, \text{ and } 4p$ orbitals; and the e representation is formed from the $3d$ and $4d$ orbitals, respectively. We neglect in this application the t_1 representation (having contributions only from $l=4$ and beyond) and the a_2 representation.

D. Augmented Green's function and the Dyson equation

While we can regard the $4s, 4p, 4d, \text{ and } 4f$ impurity basis orbitals $g_{\mu l \sigma}^{\Gamma,\lambda}(\mathbf{r})$ as perturbed versions of the $s, p, d, \text{ and } f$ orbitals, respectively, of the (impurity-centered) local host orbitals $f_l^{\Gamma,\lambda}(\mathbf{r})$, there is nothing in the unperturbed LCAO set that corresponds to the localized $3d$ states and to the hyperlocalized core states if we limit the number of host bands to the first 20 or so bands.^{35,36} Consequently, the ordinary impurity Green's-function method becomes impractical owing to the many host bands ($10^2 - 10^4$) it requires, as discussed by Lindelfelt and Zunger.³⁵ They have developed a simple method—the quasiband approach—for effectively circumventing this problem. It has and continues to be used for numerous applications.^{23,33,35,40,41} Here, for the sake of experimentation, we try the alternative Williams, Feibelman, and Lang³⁶ adspace augmentation instead of the equivalent quasiband method³⁵ for generating a variationally sufficient Green's function. According to the adspace idea of Williams *et al.*³⁶ we can perform the projection to the impurity orbital subspace using the added impurity-centered local-impurity orbitals $g_{\mu l \sigma}^{\Gamma,\lambda}(\mathbf{r})$ defined in Sec. III C. In the impurity orbital subspace we use the augmented Green's function $\tilde{G}(\epsilon)$, which is separated in two parts; one is the added orbital block which is constructed from the $3d$ orbital and the core orbitals ($1s, 2s, 2p, 3s, \text{ and } 3p$), and the second is the ordinary Green's-function block constructed from the $4s, 4p, 4d, \text{ and } 4f$ outer orbitals. The augmented *perturbed* Green's function $\tilde{G}(\epsilon)$ is defined using the matrix element of the perturbed Hamiltonian \underline{H} as

$$(\epsilon \underline{S} - \underline{H}) \tilde{G}(\epsilon) \equiv \mathbb{1}, \quad (6)$$

where \underline{S} is the overlap matrix and $\mathbb{1}$ is the unit matrix. In addition, we define the augmented *unperturbed* Green's function $\tilde{G}^0(\epsilon)$ using the unperturbed Hamiltonian \underline{H}^0 and the corresponding overlap matrix \underline{S}^0 , as

$$(\epsilon \underline{S}^0 - \underline{H}^0) \tilde{G}^0(\epsilon) \equiv \mathbb{1}, \quad (7)$$

where

$$\tilde{G}^0(\epsilon) = \begin{bmatrix} \delta_{\mu l \sigma, \mu' l' \sigma'} & 0 \\ \epsilon - \epsilon_{\mu l \sigma}^0 & \\ 0 & \underline{G}^0(\epsilon) \end{bmatrix}. \quad (8)$$

Here, $\delta_{\mu l \sigma, \mu' l' \sigma'}/(\epsilon - \epsilon_{\mu l \sigma}^0)$ represents the added 3d and core orbital block, $\epsilon_{\mu l \sigma}^0$ is defined as $\epsilon_{\mu l \sigma}^0 \equiv H_{\mu l \sigma, \mu' l' \sigma \sigma'}$, and $\tilde{G}^0(\epsilon)$ is the ordinary unperturbed Green's function of Eq. (3). The augmented perturbed Green's function $\tilde{G}(\epsilon)$ corresponding to the perturbation potential $\delta U \equiv (\underline{H} - \underline{H}^0) - \epsilon(\underline{S} - \underline{S}^0)$ is related³⁶ to $\tilde{G}^0(\epsilon)$ by Dyson's equation:

$$\tilde{G}(\epsilon) = \tilde{G}^0(\epsilon) + \tilde{G}^0(\epsilon) \delta U \tilde{G}(\epsilon). \quad (9)$$

In this equation, the one-to-one correspondence of the basis function in $\tilde{G}(\epsilon)$ and in $\tilde{G}^0(\epsilon)$ is (4s-s), (4p-p), (4d-d), and (4f-f) for the ordinary Green's-function block. In Eq. (8), we can think of $\epsilon_{\mu l \sigma}^0$ as the energy of the atomic 3d orbital or the core orbital which corresponds to the higher-energy states in the quasiband structure of Lindelfelt and Zunger.³⁵ [However, here this constant is arbitrary, since whatever constant we use for the 3d orbital and the core orbital block of \underline{H}^0 is subsequently removed when we construct the 3d and the core orbital block of the perturbation matrices $\delta U = (\underline{H} - \underline{H}^0) - \epsilon(\underline{S} - \underline{S}^0)$.]

E. Calculated properties

The *host crystal* local density of states, $n_{\Gamma, l}^{(H)}(\epsilon)$, projected on the impurity-centered local host orbitals $f_l^{\Gamma, \lambda}(\mathbf{r})$ (i.e., given in subspace I) is calculated directly from the Green's function as

$$n_{\Gamma, l}^{(H)}(\epsilon) = -\frac{1}{\pi} \sum_{\lambda} \frac{1}{M_{\lambda}} \text{Im}[\tilde{G}^0(\epsilon)]_{\Gamma, l \lambda}, \quad (10)$$

where M_{λ} is the number of members in the partner λ . The *impurity local* density of states, $n_{\Gamma, \mu l}^{\sigma}(\epsilon)$, projected on the impurity-centered local-impurity orbitals $g_{\mu l \sigma}^{\Gamma, \lambda}(\mathbf{r})$, is given similarly by

$$n_{\Gamma, \mu l}^{\sigma}(\epsilon) = -\frac{1}{\pi} \sum_{\lambda} \frac{1}{M_{\lambda}} \text{Im}[\tilde{G}(\epsilon)]_{\Gamma, \mu l \lambda}^{\sigma}. \quad (11)$$

The change in the local density of states $\Delta n_{\Gamma, \mu l}^{\sigma}(\epsilon)$ is defined as the impurity-induced piece, i.e., the difference

$$\Delta n_{\Gamma, \mu l}^{\sigma}(\epsilon) = n_{\Gamma, \mu l}^{\sigma}(\epsilon) - n_{\Gamma, l}^{(H)}(\epsilon). \quad (12)$$

The change in the charge density $\Delta \rho^{\sigma}(|\mathbf{r}|)$ is similarly defined as

$$\Delta \rho^{\sigma}(|\mathbf{r}|) = \sum_{\Gamma, \mu l} d\Gamma [\rho_{\Gamma, \mu l}^{\sigma}(|\mathbf{r}|) - \rho_{\Gamma, l}^{(H)}(|\mathbf{r}|)], \quad (13)$$

where $\rho_{\Gamma, l}^{\sigma}$ is the perturbed charge density for spin σ and $\rho_{\Gamma, l}^{(H)}$ is the unperturbed (and unpolarized) host charge density. $\rho_{\Gamma, l}^{\sigma}$ and $\rho_{\Gamma, l}^{(H)}$ are calculated by projecting the density of states on the corresponding local orbitals, i.e.,

$$\rho_{\Gamma, \mu l}^{\sigma}(|\mathbf{r}|) = \int_{-\infty}^{\epsilon_F} n_{\Gamma, \mu l}^{\sigma}(\epsilon) |F_{\mu l \sigma}^{(I)}(|\mathbf{r}|)|^2 d\epsilon, \quad (14)$$

and

$$\rho_{\Gamma, l}^{(H)}(|\mathbf{r}|) = \int_{-\infty}^{\epsilon_F} n_{\Gamma, l}^{(H)}(\epsilon) |F_l^{(H)}(|\mathbf{r}|)|^2 d\epsilon. \quad (15)$$

Here, $F_{\mu l \sigma}^{(I)}$ and $F_l^{(H)}$ are the impurity and host radial orbitals of Eqs. (4) and (2), respectively, ϵ_F is the Fermi energy, and $d\Gamma$ denotes the number of the partner in the Γ representation.

The number of electrons occupying bound states in the band gap in the impurity orbital subspace is defined as

$$Q_{\mu l}^{\sigma} = n_b |C_{\mu l}^{\sigma}|^2, \quad (16)$$

per orbital, where n_b denotes the occupation number of the bound states, and the impurity wave function in subspace I is

$$\psi^{(I)}(\mathbf{r}) = \sum_{\mu l \lambda, \sigma} C_{\mu l}^{\sigma} g_{\mu l \sigma}^{\Gamma, \lambda}(\mathbf{r}). \quad (17)$$

The normalization condition of Eq. (17) in the whole space is

$$-\langle \psi^{(I)}(\mathbf{r}) | \delta U \frac{\partial \tilde{G}^0(\epsilon)}{\partial \epsilon} \delta U | \psi^{(I)}(\mathbf{r}) \rangle = 1. \quad (18)$$

The total change in the number of states for the irreducible representation Γ below the given energy ϵ (i.e., the phase shift) $\delta_{\Gamma}^{\sigma}(\epsilon)$ is given by

$$\delta_{\Gamma}^{\sigma}(\epsilon) = -\frac{1}{\pi} \text{Im} \ln \det ||1 - \tilde{G}^0(\epsilon) \delta U||_{\Gamma}^{\sigma}. \quad (19)$$

Since $\delta_{\Gamma}^{\sigma}(\epsilon)$ gives the information in the whole space, we can obtain the information on subspace II combined with the information from $\Delta n_{\Gamma, \mu l}^{\sigma}(\epsilon)$ in the impurity orbital subspace without expanding the perturbation to the surrounding host silicon shells.

The total change in the magnetic moment ΔM induced by the impurity atom is calculated from the change $N^+(\epsilon_F)$ and $N^-(\epsilon_F)$ in the number of states for each spin below the Fermi level ϵ_F by

$$\Delta M = N^+(\epsilon_F) - N^-(\epsilon_F). \quad (20)$$

$N^{\sigma}(\epsilon_F)$ is related to the phase shift $\delta_{\Gamma}^{\sigma}(\epsilon_F)$ of Eq. (19) through

$$N^{\sigma}(\epsilon_F) = \sum_{\Gamma} d\Gamma \delta_{\Gamma}^{\sigma}(\epsilon_F). \quad (21)$$

The charge neutrality conditions, i.e., the Friedel sum rule, requires

$$\Delta Z = N^+(\epsilon_F) + N^-(\epsilon_F), \quad (22)$$

where ΔZ is the change in the charge. In the case of an interstitial impurity we have $\Delta Z = Z$, where Z denotes the atomic number of the impurity atom in the case of neutral impurity.

The impurity-induced change in the local magnetic moment Δm (i.e., in the *impurity* orbital subspace) is related to the change in the local density of states $\Delta n_{\Gamma, \mu l}^{\sigma}(\epsilon)$ of Eq. (12) by

$$\Delta m = \sum_{\Gamma, \mu l} [p_{\Gamma, \mu l}^{\pm}(\epsilon_F) - p_{\Gamma, \mu l}^{\mp}(\epsilon_F)], \quad (23)$$

where

$$p_{\Gamma, \mu l}^{\sigma}(\epsilon_F) = d\Gamma \int_{-\infty}^{\epsilon_F} \Delta n_{\Gamma, \mu l}^{\sigma}(\epsilon) d\epsilon, \quad (24)$$

denotes the occupation number of the μl component of the Γ representation with spin σ in the impurity orbital subspace. Since ΔM gives the total magnetic moment in the *whole space*, and Δm gives the local magnetic moment in the *impurity orbital subspace*, we can find out how much of the spin density is expanded through the crystal using the difference between ΔM and Δm .

The effective local orbital occupation number $N_{\mu l}(\epsilon)$ in

the valence band is defined as

$$N_{\mu l}(\epsilon) = \sum_{\Gamma, \sigma} d\Gamma \int_{-\infty}^{\epsilon} \Delta n_{\Gamma, \mu l}^{\sigma}(\epsilon') d\epsilon' . \quad (25)$$

F. Impurity hyperfine field and isomer shift

The main contributions to the hyperfine field of a magnetic impurity⁴² are (i) the contribution from the Fermi contact interaction (including Fermi direct contact interaction and core polarization), (ii) the contribution from the interaction with the orbital magnetic moment of the electrons, and (iii) the contribution from the dipole-dipole interaction. Contribution (iii) is usually as small as⁴² a few kilogauss (kG), and will be ignored here. The hyperfine field from the contribution (i), $H_{\text{hf}}^{(i)}$, is related to the spin density at the nucleus⁴³ $\delta\rho(0)$ by

$$H_{\text{hf}}^{(i)} = \frac{8\pi}{3} \mu_B \delta\rho(0) = 524.2 \delta\rho(0) \text{ kG} , \quad (26)$$

where μ_B is the electron Bohr magneton, and $\delta\rho(0)$ is the spin density at the nucleus (in a.u.) defined by

$$\delta\rho(\mathbf{r}) = \Delta\rho^+(\mathbf{r}) - \Delta\rho^-(\mathbf{r}) , \quad (27)$$

where the impurity-induced change in the charge density for spin σ , i.e., $\Delta\rho^{\sigma}(\mathbf{r})$ is defined in Eq. (13). The hyperfine field from contribution (ii), $H_{\text{hf}}^{(ii)}$, is related⁴⁴ to the g shift Δg and the average of r^{-3} over the orbital $\langle 1/r^3 \rangle_{\text{av}}$ at $\epsilon = \epsilon_F$ as

$$H_{\text{hf}}^{(ii)} = 2\mu_B \Delta g S \langle 1/r^3 \rangle_{\text{av}} = 125 \Delta g S \langle 1/r^3 \rangle_{\text{av}} \text{ kG} . \quad (28)$$

The isomer shift of iron as observed in the Mössbauer effect⁴⁵ is given by

$$\begin{aligned} \Delta_{\text{IS}} &= \frac{2\pi e^2 Zc}{3E_{\gamma}} [|\phi_a(0)|^2 - |\phi_s(0)|^2] \Delta \langle r_n^2 \rangle \\ &= -0.157 [|\phi_a(0)|^2 - |\phi_s(0)|^2] \text{ (in mm/sec)} , \quad (29) \end{aligned}$$

where E_{γ} denotes the energy of the resonant gamma ray (14.4 keV), Z is the nuclear charge, $\Delta \langle r_n^2 \rangle$ is the change in the second moment of the nuclear charge distribution accompanying nuclear excitation (in units of $10^{-3} f_m^2$), $|\phi_s(0)|^2$ is the electron charge density of source nuclei at the nucleus, and $|\phi_a(0)|^2$ is the charge density of the absorber (both in a.u.). In Eq. (29), we use⁴⁶ $\Delta \langle r_n^2 \rangle = -14.3 \times 10^{-3} f_m^2$, which is determined from the Mössbauer experiment of the free ion (Fe^0 and Fe^+) in Xe and the density of the free atom using the Dirac-Fock-Slater method.⁴⁶

G. Perturbation potential and the self-interaction problem

Most electronic structure calculations on transition atom impurities in semiconductors^{23,33-35,40,41,47-51} were performed within the local-spin-density formalism (LSD),⁵² implemented either in an extended-crystal Green's-function approach^{23,33-35,40,41,47} or within finite-cluster models.⁴⁸⁻⁵¹ Involving a local statistical approximation to exchange and correlation, the local-spin-density approximation, much like its predecessor, the Thomas-

Fermi model (but unlike the Hartree-Fock model) involves an unphysical interaction of each spin orbital with itself⁵³ (self-interaction). This sets up spurious self-Coulomb repulsion, self-exchange, and self-correlation interactions. Whereas these terms have a vanishing effect on extended delocalized states, they may have a significant effect on localized states. Such is the case for isolated transition atoms, where a self-interaction free model shows⁵³ that, relative to LSD, (i) the $3d$ orbitals move to substantially more negative energies (thereby increasing the s - d separation); (ii) the $3d$ orbitals become more localized, whereas the non- d valence orbitals become more expanded; (iii) the exchange splitting between spin-up and spin-down $3d$ orbitals increases; (iv) the contact spin density at the nucleus is increased; (v) the total exchange energy becomes more negative, whereas the total correlation energy becomes less negative; and (vi) the total ground-state density becomes more localized. Whereas self-interaction corrections were applied recently with substantial success to atoms,⁵³ molecules,⁵⁴ and solids,^{53,55} showing significant improvements relative to the uncorrected formalism, until recently^{33(a)} they were not considered for impurities. Of particular interest here are the interstitial $3d$ impurities that are likely to maintain their localized atomiclike characteristics more than the substitutional impurities, as the former have only weak bonds with the (chemically saturated) host ligand atoms. Here, application of the uncorrected local-density formalism within a 17-atom cluster with hydrogen terminators and spherically symmetrized atomic potentials⁵⁰ has first shown reasonable results. In particular, the high-spin ($S = \frac{3}{2}$) ground state of Si:Fe^+ was correctly predicted. However, subsequent calculations^{33(a)} have indicated that this success resulted primarily from the underestimation of the crystal-field (CF) splitting ($\Delta_{\text{CF}} = 0.025$ eV was obtained in Ref. 50) attendant upon the spherical approximation to the crystal potential.⁵⁰ When nonspherical components were introduced self-consistently,^{33(a)} Δ_{CF} increased and outweighed the exchange splitting Δ_x , producing thereby a low-spin ground state, in contrast with experiment. It was further shown^{33(a)} that, whereas the local-spin-density formalism, when carried out with the full-potential anisotropy, does not describe correctly the symmetry of the many-electron ground state (much like the situation in free atoms), a self-interaction free model produces the correct result. Since, however, the earlier self-interaction corrected (SIC) were applied perturbatively,^{33(a)} it seems to us to be of interest to apply them now nonperturbatively (i.e., self-consistently) and examine the consequences of this approach. To this end, we have carried out self-consistent spin-polarized calculations for Si:Fe^0 and Si:Fe^+ using the impurity Green's-function approach with general potentials and the self-interaction correction. We discuss below the construction of the perturbation potential in this approach.

For the case of LSD, the spin-polarized perturbation potential $\Delta V_{\text{LSD}}^{\sigma}$ is given by

$$\begin{aligned} \Delta V_{\text{LSD}}^{\sigma}[\bar{\rho}] &= -\frac{Z}{r} + V_{e-e}[\Delta\bar{\rho}] + V_{\text{xc}}^{\sigma}[\bar{\rho}^{(H)} + \Delta\bar{\rho}^{\sigma}] \\ &\quad - V_{\text{xc}}^{\sigma}[\bar{\rho}^{(H)}] , \quad (30) \end{aligned}$$

where V_{e-e} and V_{xc}^σ are, respectively, the electron-electron ($e-e$) and exchange-correlation (xc) potentials in LSD (we use the Ceperley-Adler exchange correlation as given by Perdew and Zunger⁵³), $\bar{\rho}^{(H)}$ denotes the charge density of the host crystal, and $\Delta\bar{\rho}^\sigma$ denotes the charge perturbation for spin σ . $\bar{\rho}_I$ is the total impurity (I) charge density defined by $\bar{\rho}_I = \bar{\rho}^{(H)} + \Delta\bar{\rho}(|\mathbf{r}|)$. Bars indicate that the charge density is computed self-consistently from the LSD potential. For the case of SIC-LSD, we have⁵³

$$\Delta V_{\text{SIC-LSD}}^{\mu\sigma}[\rho_I] = \Delta V_{\text{LSD}}^\sigma[\rho_I] - \delta V_{\text{SIC}}^{\mu\sigma}, \quad (31)$$

where $\Delta V_{\text{LSD}}^\sigma[\rho_I]$ is the LSD perturbation potential computed from the density $\rho_I(r)$ [self-consistent for SIC potentials, rather than $\bar{\rho}_I(r)$ as in Eq. (30)], and $\delta V_{\text{SIC}}^{\mu\sigma}$ is the orbital-dependent self-interaction correction, i.e., Refs. 53 and 56,

$$\delta V_{\text{SIC}}^{\mu\sigma} = V_{e-e}[q_{\mu\sigma} | F_{\mu\sigma}^{(I)}|^2] + V_{xc}^+[q_{\mu\sigma} | F_{\mu\sigma}^{(I)}|^2]. \quad (32)$$

It consists of a self-Coulomb (first-term) and a self-exchange-correlation (second-term) correction. Here, $q_{\mu\sigma}$ are the occupation numbers (used here as 1 for occupied spin-orbitals and 0 otherwise) and $F_{\mu\sigma}^{(I)}$ are the impurity-centered radial orbitals of Eq. (4). We compute $F_{\mu\sigma}^{(I)}(|\mathbf{r}|)$ by averaging over the degenerate partner orbitals before filling the states. We start with some trial orbital set $\{F_{\mu\sigma}^{(I)}(|\mathbf{r}|)\}$ and use it to compute the perturbation matrix elements in this local orbital representation. Using it, we solve Dyson's equation [Eq. (9)] to obtain the perturbed Green's function from which we obtain the local density of states $n_{\Gamma,\mu\sigma}^\sigma(\epsilon)$ in Eq. (11) for all representations $\Gamma = a_1, e, \text{ and } t_2$. Projecting it (as well as the unperturbed host density of states) on the local orbitals $F_{\mu\sigma}^{(I)}(|\mathbf{r}|)$ and summing over all occupied states, we obtain the impurity-induced change in the charge density $\Delta\rho^\sigma(|\mathbf{r}|)$ of Eq. (13). This is then used in Eqs. (30) or (31) to construct the new perturbation potential. Together with the (fixed) host crystal potential $V^{(H)}(|\mathbf{r}|)$, this gives the effective impurity potential used to solve for the new impurity local orbitals $\{F_{\mu\sigma}^{(I)}(|\mathbf{r}|)\}$ in the effective impurity Schrödinger equation of Eq. (5). The process is repeated iteratively until self-consistency in $\Delta V(|\mathbf{r}|)$ (equal or better than 0.8 mRy) is obtained. We use the Jacobian update method⁵⁷ to obtain very rapid convergence.

The main approximations in our calculation involve the neglect of space correlation energies and of lattice distortions. Recent calculations of the multiplet energies for 3d impurities in semiconductors³⁰ suggest that most (but not all) of the multiplet energy in exchange derived and, hence, well represented by a spin-polarized calculation. The use of unrelaxed lattice geometries seems justified since (i) experimentally, there is no measurable static Jahn-Teller distortion¹⁸ in Si:Fe⁺, (ii) there is an isotropic g shift and hyperfine coupling constant,¹⁸ and, theoretically (iii) Lindefelt and Zunger²³ find small ($\sim 3\%$) symmetry conserving distortion based upon their nonmagnetic quasiband crystal-field calculation.

IV. RESULTS

A. Unperturbed Green's function

Figure 2(a) depicts the total host crystal density of states and Figs. 2(b)–2(h) show the ordinary unperturbed Green's function $\underline{G}^0(\epsilon)$ of Eq. (3), including its real part and imaginary part (shaded). We note that $\text{Im}G_{s,s}^{0,a_1}(\epsilon)$ [solid lines in Fig. 2(b)] has three peaks inside the valence band. The first peak at $E_v - 11$ eV is constructed primarily from the tails of the s orbital on the neighboring silicon atoms. The second peak at $E_v - 7$ eV is composed of the tails of s and p orbitals. In contrast, the third peak at $E_v - 4$ eV is constructed mainly from the tails of the p orbitals of the six octahedrally coordinated second-neighbor silicon atoms (whose distance from the tetrahedral interstitial impurity site is 1.15 times the nearest-neighbors distance). In the imaginary parts of the $\underline{G}^0(\epsilon)$ for the d orbital component in the t_2 and e representations [Figs. 2(f) and 2(h), respectively] we note that the amplitude of $\text{Im}G_{d,d}^{0,e}(\epsilon)$ [Fig. 2(h)] is larger than that of $\text{Im}G_{d,d}^{0,t_2}(\epsilon)$ [Fig. 2(f)] at $E_v - 4$ eV to $E_v - 1$ eV region. Note that $\text{Im}G_{d,d}^{0,t_2}(\epsilon)$ is constructed mainly from the tails of the p orbitals on the *four* tetrahedrally coordinated nearest neighbors; on the other hand, $\text{Im}G_{d,d}^{0,e}(\epsilon)$ at $E_v - 1$ eV is constructed mainly from the tails of the p orbitals on the *six* octahedrally coordinated second-neighbor silicon atoms. The larger coordination of the second neighbors outweighs the difference in the distance between the impurity site and its neighbors. Because the amplitude of $\text{Im}G_{d,d}^{0,e}(\epsilon)$ is larger than that of $\text{Im}G_{d,d}^{0,t_2}(\epsilon)$, we expect that the 3d impurity orbital in the e representation can have a larger hybridization with the tails of the sp^3 hybrid orbitals on the surrounding silicon atoms compared with the t_2 states. This is the key to understanding the crystal-field splitting between the e and t_2 representations of the 3d impurity states at the tetrahedral interstitial site, as will be discussed in Sec. V.

We also note that the representation-by-representation local density of states of Si, projected at the interstitial site [Figs. 2(b)–2(h)] is significantly different from the distribution of states given by a small silicon cluster model.⁵⁰ Since the impurity states of an interstitial 3d atom in silicon evolve from the hybridization of an atomic 3d orbital with these distributions, it is not surprising that our Green's-function calculation gives substantially different results than the cluster calculation (see also Sec. V E). The fundamental reason for this difference is that a small cluster model, involving a hierarchy of ligand shells (i.e., first- and second-nearest neighbors to the tetrahedral interstitial site⁵⁰) does not represent correctly the hierarchy of peaks in the local density of states (Fig. 2). Stated simply, the host states of symmetries e and t_2 (relative to the interstitial site) are misplaced in the small cluster model relative to the continuum representation (compare Fig. 3 in Ref. 50 to our Fig. 2), leading to a different pattern of hybridization. We will return to this point in Sec. V E.

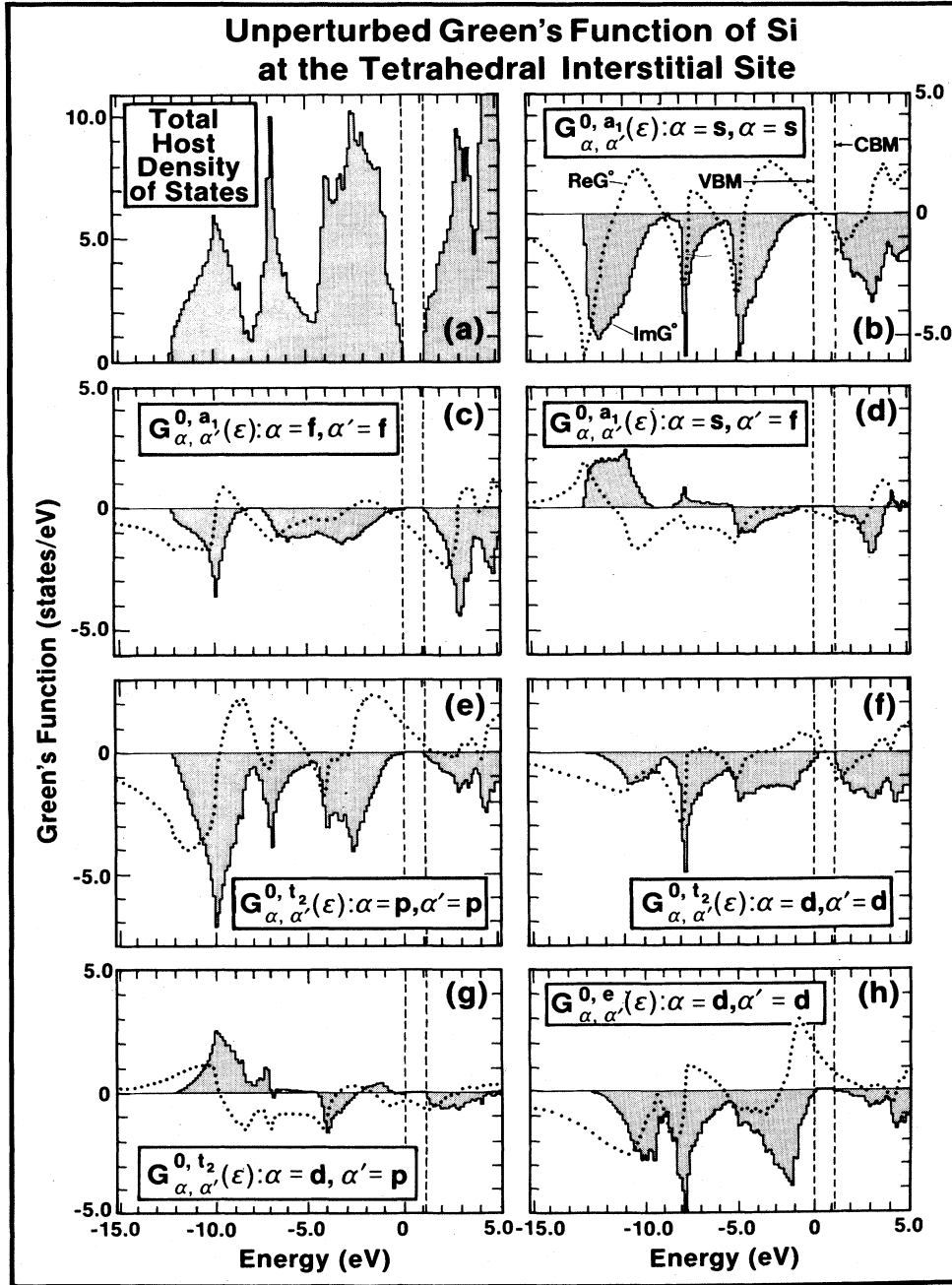


FIG. 2. (a) Total host density of states calculated by the LCAO method, and (b)–(h) the unperturbed ordinary Green's function $G_{\alpha, \alpha'}^0(\epsilon)$, for the representation $\Gamma = a_1, e$, and t_2 and the orbital components $\alpha = s, p, d$, and f . The dotted (solid) line shows the real (imaginary) parts of the Green's function. The vertical horizontal lines denote the band edges.

B. Impurity levels of Si:Fe⁰ in the SIC-LSD approach

Figure 3 shows the phase shifts $\delta_{\Gamma}^{\sigma}(\epsilon)$ [defined in Eq. (19)] which gives the change in the number of states of the irreducible representation Γ below a given energy ϵ in the whole space (not just in the impurity orbital subspace) for each spin σ . Figures 4, 5, and 6 show the change within the impurity orbital subspace $\Delta n_{\Gamma, \alpha}^{\sigma}(\epsilon)$ in the local density of states for each orbital component ($\alpha = \mu l$), spin σ and

representation $\Gamma = a_1$ (Fig. 4), e (Fig. 5), and t_2 (Fig. 6), as given in the SIC-LSD formalism. The number of electrons $Q_{\mu l}^{\sigma}$ [cf., Eq. (16)] in gap bound states in the impurity orbital subspace for each $\mu l \sigma$ spin orbital, is also indicated in these figures. Figure 7 summarizes schematically these results as an energy-level diagram: it shows the peak energy and width at half value in the local density of states in impurity orbital subspace. For the a_1 representation, the three peaks of $\delta_{a_1}^{\sigma}(\epsilon)$ [i.e., Figs. 3(a) and 3(b)] in-

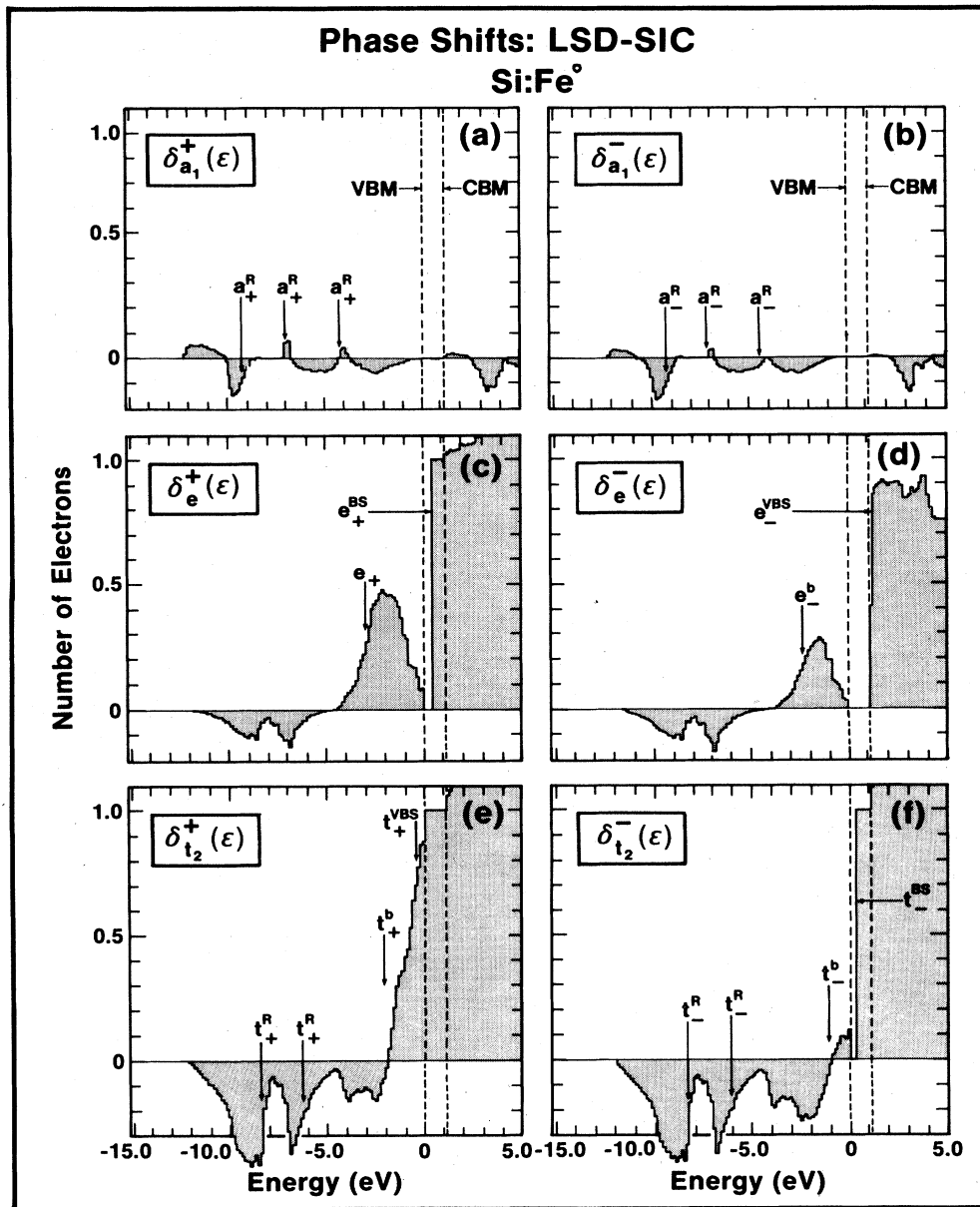


FIG. 3. Phase shift, $\delta_{\Gamma}^{\sigma}(\epsilon)$, of Si:Fe⁰ calculated in the LSD-SIC method for spin σ (+ or -) and representation $\Gamma = a_1, e$, and t_2 , showing the bonding (b), antibonding (a), resonances (R), virtual bound states (VBS), and bound states (BS).

side the valence band correspond to the resonant states (R) caused by the attractive impurity potential in a_1 representation. These resonant states are delocalized in the impurity orbital subspace, as there is little charge in $\Delta n_{a_1,4s}^{\sigma}(\epsilon)$ and $\Delta n_{a_1,4f}^{\sigma}(\epsilon)$ (cf., Fig. 4) at the vicinity of the resonant energy in the impurity orbital subspace. For the e representation, a large hybridization between the impurity $3d$ orbital and the tails of the sp^3 hybrid orbitals of the surrounding silicon atoms gives rise to the bonding (b) states [i.e., e_{σ}^b in Figs. 7, 3(c), and 3(d)] inside the valence band and to the antibonding (a) bound states (BS) [i.e., e_{σ}^a in Fig. 7 and e_{σ}^{BS} in Fig. 3(c)] being pushed up

into the band gap. The bonding states (e_{σ}^b) are mainly constructed from the $3d$ orbital. The antibonding BS in the band gap are more extended than the e_{σ}^b states. For the t_2 representation, we find the two delocalized resonant (R) states [i.e., t_{σ}^R in Figs. 7, 3(e), and 3(f)] inside the valence band. In addition, we also find the bonding (b) valence-band states [i.e., t_{σ}^b in Figs. 7, 3(e), and 3(f)] and the antibonding virtual bound states (VBS) (i.e., t_{σ}^{VBS} in Fig. 3) at the top of the valence band for up-spin states. The bonding states (t_{σ}^b) in Figs. 3(e) and 3(f) are constructed mainly from the $3d$ orbitals, whereas the antibonding states [i.e., t_{σ}^{BS} in Fig. 3(f)] have less $3d$ charac-

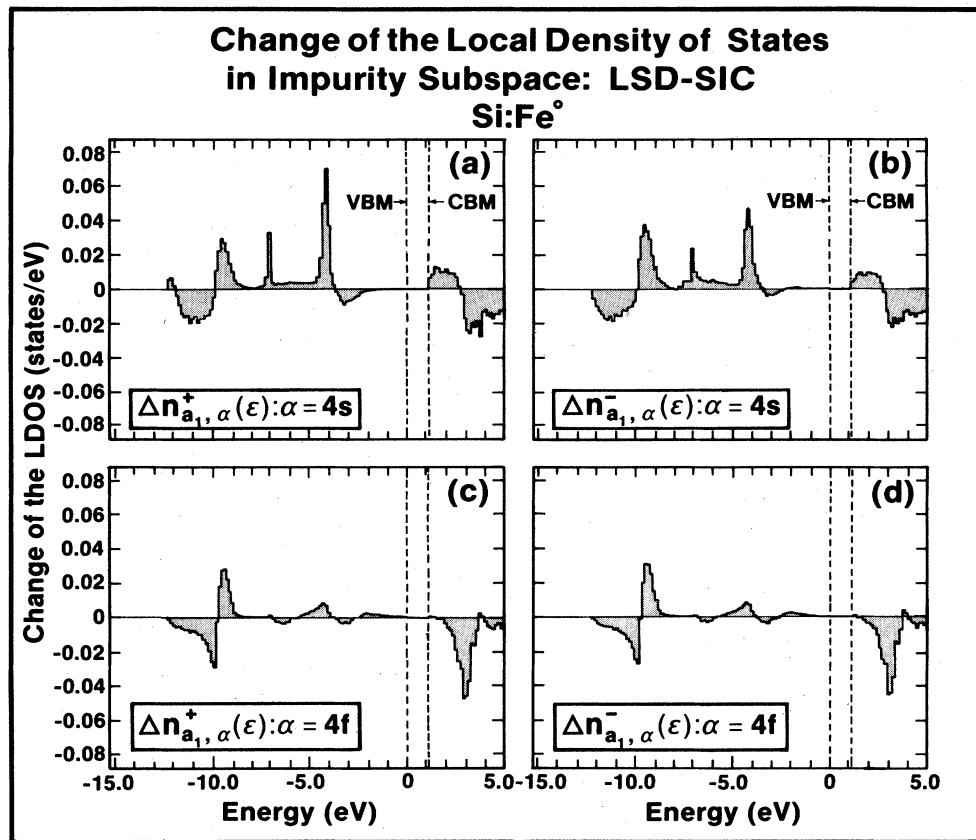


FIG. 4. Change $\Delta n_{\Gamma,\alpha}^{\sigma}(\epsilon)$ of the local density of states of Si:Fe⁰ in SIC-LSD for spin σ (+ or -) and the representation $\Gamma = a_1$. We show each orbital component: $\alpha = 4s$ and $4f$.

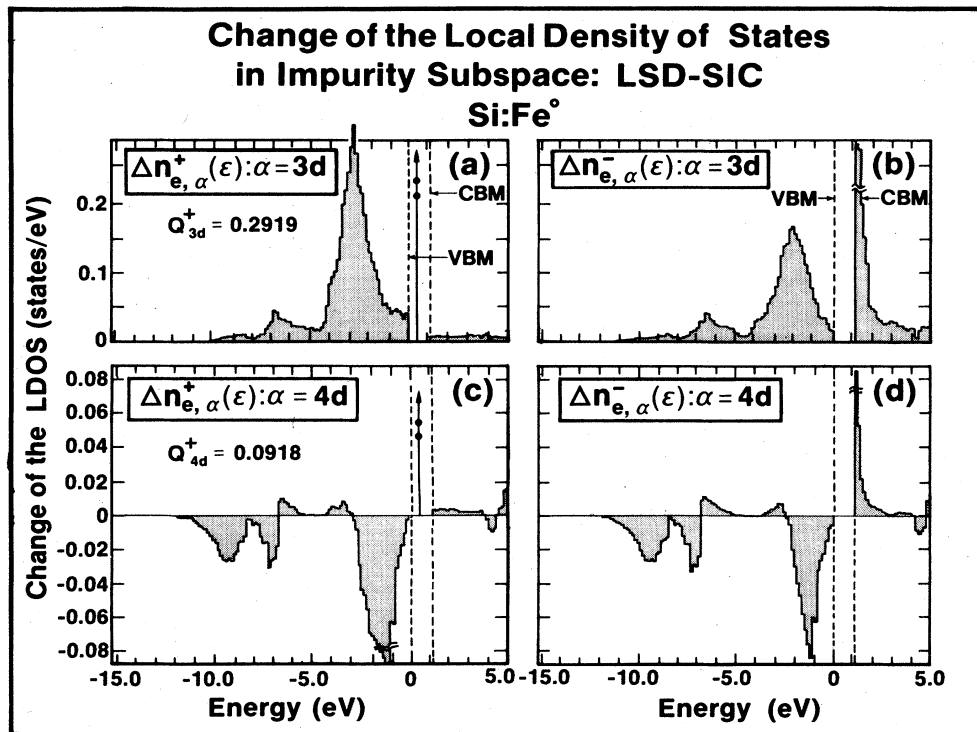


FIG. 5. Change $\Delta n_{\Gamma,\alpha}^{\sigma}(\epsilon)$ of the local density of states of Si:Fe⁰ in SIC-LSD for spin σ (+ or -) and the representation $\Gamma = e$. We show each orbital component: $\alpha = 3d$ and $4d$.

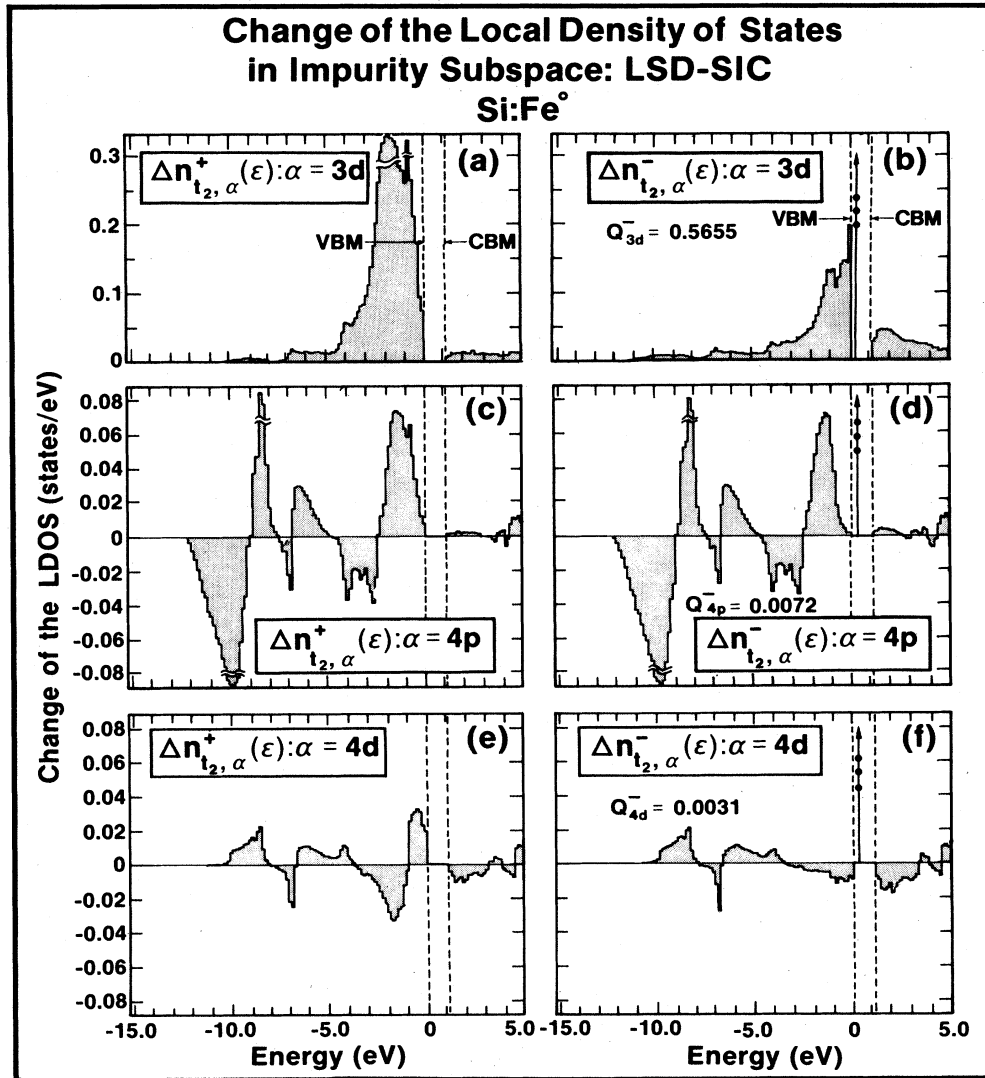


FIG. 6. Change $\Delta n_{\Gamma, \alpha}^{\sigma}(\epsilon)$ of the local density of states of Si:Fe^0 in SIC-LSD for spin σ (+ or -) and the representation $\Gamma = t_2$. We show each orbital component: $\alpha = 3d, 4p$, and $4d$.

ter. For down-spin states, because of the exchange splitting this antibonding state is found in the band gap as a bound state [i.e., (t_{σ}^{BS}) in Fig. 3(f)]. We define the exchange splitting Δ_x^e as the difference between the down-spin and up-spin one-electron orbital energies which carry most of the impurity $3d$ character. For the e representation, we find these to be the bonding e_{\pm}^b orbitals, hence $\Delta_x^e = \epsilon(e_{-}^b) - \epsilon(e_{+}^b)$. For the t_2 representation we similarly have $\Delta_x^t = \epsilon(t_{-}^t) - \epsilon(t_{+}^t)$. Note that other definitions are possible too, e.g., one would have used the splitting between the antibonding t_{\pm}^a orbital energies as a measure for Δ_x . However, these orbitals are not the counterparts of the atomic d_{\pm} orbitals which define the exchange splitting in the atomic limit. A third definition, of the “effective exchange energy” is possible too (i.e., differences in total energies required to flip a spin in a given representation) but will not be used in the present work. We define the crystal-field splitting as the difference $\Delta_{\text{CF}} \equiv \epsilon(e_{+}^a)$

$-\epsilon(t_{+}^a)$ (e.g., Figs. 7 and 3). The width in the local density of states of e_{σ}^b is larger than that of t_{σ}^b [cf., Figs. 5(a), 5(b), 6(a), 6(b) and 7], because the stronger hybridization induces a larger width in the local density of states. We find Δ_x to be 0.7 eV and the crystal-field splitting Δ_{CF} is 0.8 eV. The ratio between the exchange splitting and the crystal-field splitting, $\Delta_x/\Delta_{\text{CF}}$, is 0.88, i.e., our results suggest that crystal-field effects surpass exchange effects in the neutral charge state.

The three impurity-induced a_1 valence-band resonances (i.e., Figs. 3 and 7) are largely delocalized and hostlike: The total change in the number of states is 0.1–0.2 near the energy of these resonances. On the other hand, the change of the local density of states (LDOS) in this energy region in *impurity orbital subspace* is only 0.01–0.02. These resonances contribute a small local magnetic moment $\Delta m_{a_1}^{\text{VB}} = 0.01 \mu_B$. We find broader, bonding e_{σ}^b states in the valence band, which peak around $E_v - 2.8$ eV

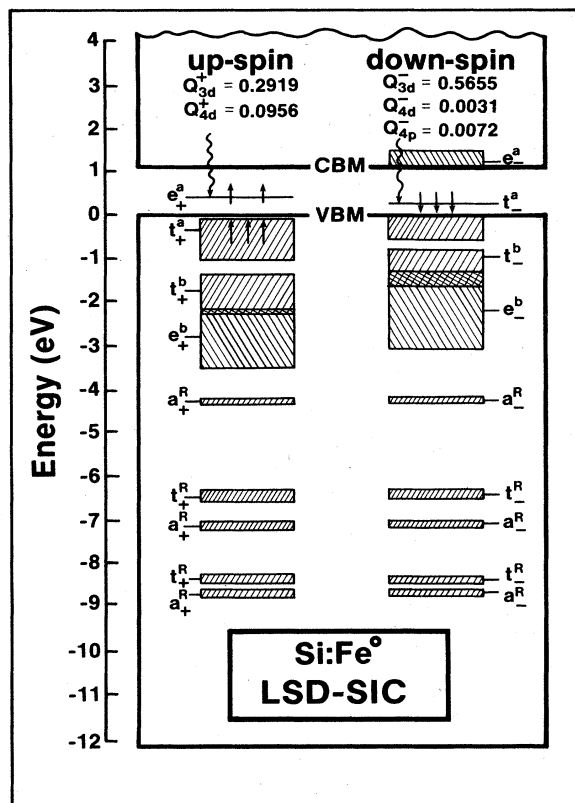


FIG. 7. Calculated impurity-induced levels and the width of the half value of the peak for Si:Fe⁰ in SIC-LSD, showing the bonding (*b*), antibonding (*a*), resonance (*R*), up-spin (+), and down-spin (−) levels.

[i.e., Figs. 5(a) and 5(b)] and carry a local magnetic moment of $\Delta m_e^{\text{VB}} = 0.78\mu_B$. Their antibonding (up-spin) counterpart is in the gap at $E_v + 0.44$ eV and contribute $\Delta m_e^{\text{gap}} = 0.38\mu_B$. The t_2 states appear first as two deep resonances peaking at $E_v - 8.5$ eV and $E_v - 6.5$ eV, then a bonding resonance at $E_v - 1.8$ eV whereas the antibonding states (i.e., Figs. 3 and 6) appear just near the valence-band maximum (VBM), contributing together a local magnetic moment of $\Delta m_{t_2}^{\text{VB}} = 0.81\mu_B$. The down-spin t_2 state at $E_v + 0.26$ eV is occupied in the neutral ground state by three electrons and contributes a negative local magnetic moment of $\Delta m_{t_2}^{\text{gap}} = -0.58\mu_B$.

To summarize, we find the most ($\sim 80\%$) of the $3d$ amplitude in the impurity orbital subspace in Si:Fe⁰ exists as localized resonance inside the valence band, dominating the magnetism ($\Delta m^{\text{VB}} = 1.61\mu_B$ versus $\Delta m^{\text{gap}} = -0.19\mu_B$), and the impurity charge (6.76 out of 8.0 valence electrons are in the valence band, and 18 are in the core). We will see that this coexistence, in a similar energy range, of localized impurity states with itinerant host states with which charge can be exchanged without surpassing an excitation barrier, is the key to the remarkable stability of various charge states.

C. Impurity levels of Si:Fe⁰ in the LSD approach

Figure 8 shows the phase shifts $\delta_{\Gamma}^{\sigma}(\epsilon)$ given by Eq. (19) in the LSD formalism. Figure 9 shows the change of the local density of states $\Delta n_{\Gamma, \alpha}^{\sigma}(\epsilon)$ of orbital component $\alpha = 3d, 4s$, and $4p$ for each spin $\sigma = \pm$ and representation $\Gamma = a_1, e$, and t_2 in the impurity orbital subspace. Figure 10 shows the peak energy and the width at half value of the local density of states in the impurity orbital subspace. The overall feature of the calculated results is qualitatively similar to that obtained in the SIC-LSD method (i.e., Sec. IV B), but the exchange splitting Δ_x in the LSD is about 0.3 eV, less than half its size in the SIC-LSD calculation ($\Delta_x = 0.7$ eV). The crystal-field splitting Δ_{CF} is now 0.9 eV, i.e., a little larger than that in the SIC-LSD (i.e., $\Delta_{\text{CF}} = 0.8$ eV). The ratio between the exchange splitting and the crystal-field splitting, $\Delta_x/\Delta_{\text{CF}}$, is 0.33, considerably smaller than that in the SIC-LSD result (i.e., $\Delta_x/\Delta_{\text{CF}} = 0.88$).

D. Orbital configurations and moment distributions

The total impurity occupation ΔZ in the whole space is given by Eq. (22). From the phase shifts $\delta_{\Gamma}^{\sigma}(\epsilon)$ shown in Figs. 3 and 8 we calculate ΔZ and divide it into two contributions: from the valence band denoted as VB states (including here occupied core states) and from the gap states denoted as gap. These are shown in Table II for the SIC-LSD and LSD (they are identical in both cases). We find that ΔZ satisfies the Friedel sum rule ($\Delta Z = 26.0$) and that the total charge is shared in a 1:3 proportion between the e and t_2 states [total representation occupations of (core)^{18.0} $a_1^{0.0}e^{2.0}t_2^{6.0}$]. Hence, there are five gap electrons (two in e with spin-up and three in t_2 with spin-down), contributing a total magnetic moment of $-1\mu_B$.

The local-impurity orbital occupation number $N_{\mu l}(\epsilon)$ in the impurity orbital subspace is given by Eq. (25). We calculate $N_{\mu l}(\epsilon)$ and divide it into the same two contributions: valence band and gap states. They are shown in Tables III and IV for the SIC-LSD and LSD cases, respectively. We find the total charge in the *impurity orbital subspace* to be $p = 25.7236e$ in the SIC-LSD case and $p = 25.4448e$ in the LSD case. Whereas the total charge ΔZ in the *whole space* is 26.0, the charge in the impurity orbital subspace is less than ΔZ . Therefore, locally, iron has a small positive net charge (nuclear charge minus electronic charge) $Q_{\text{net}} = 0.276e$ in SIC-LSD and $Q_{\text{net}} = 0.555e$ in LSD, indicating a small Fe-to-Si ionic charge transfer. We hence find that 99% (98%) of the electron charge [i.e., $(1 - Q_{\text{net}}/\Delta Z)100$] is localized in the impurity orbital subspace in the SIC-LSD (LSD) models. We find that, in agreement with the nonmagnetic quasi-band crystal-field (QBCF) calculation³³ and with Ludwigh and Woodbury,^{18(a)} a population analysis of the electronic charge (Tables III and IV) reveals that the s electrons are largely transferred into d orbitals [effective orbital configuration calculated from Eq. (25):

$$(\text{core})^{18.0}4s^{0.06}4p^{-0.13}3d^{8.18}4d^{-0.38}4f^{-0.00}$$

for SIC-LSD and

$$(\text{core})^{18.0}4s^{-0.11}4p^{0.08}3d^{7.91}4d^{-0.43}4f^{-0.00}$$

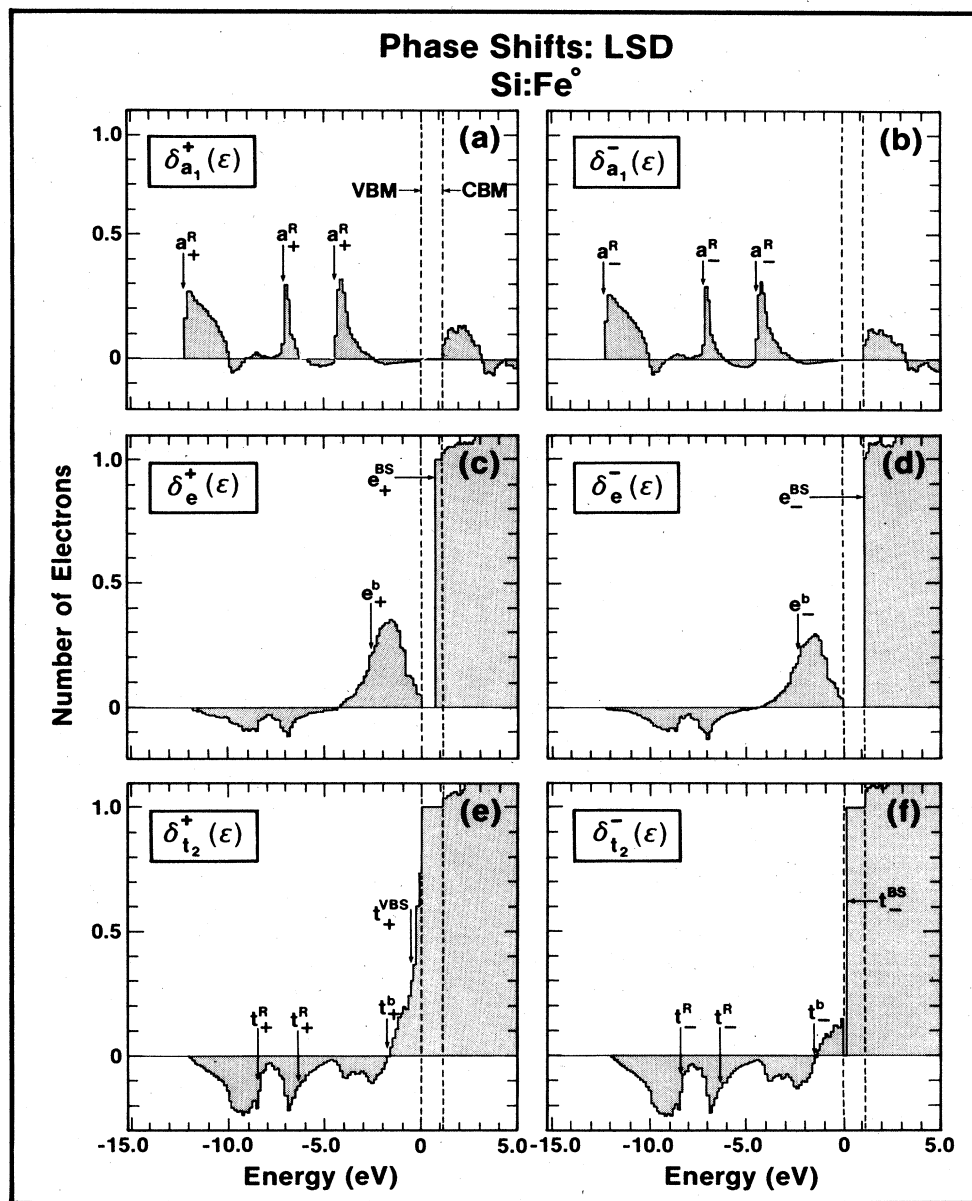


FIG. 8. Phase shift, $\delta_{\Gamma}^{\sigma}(\epsilon)$, of Si:Fe⁰ calculated in the LSD method for spin σ (+ or -) and representations $\Gamma = a_1, e,$ and t_2 , showing the bonding (b), antibonding (a), resonance (R), virtual bound states (VBS), and bound states (BS).

for LSD]. This $s \rightarrow d$ population inversion decreases the effective size of the atom (as extended s states are converted to more localized d states) without converting it into ion. Therefore, this suggests a simple chemical reason for its fast diffusivity and low solubility³⁻⁶—the occurrence of a rather small diffusing species.

The total magnetic moment ΔM in the whole space is given by Eq. (20). From the phase shifts $\delta_{\Gamma}^{\sigma}(\epsilon)$ shown in Figs. 3 and 8 we calculate ΔM and divide it into a valence-band contribution and a gap contribution (Table II). In the calculation of the magnetic moment, we assume the g factor to be 2.0 for the $3d$ states of iron impurity. Hence, not surprisingly, we find a total moment

$\Delta M = 2.0\mu_B$ per iron impurity.

The local magnetic moment Δm in the impurity orbital subspace is given by Eq. (23). From the change of the local density of states $\Delta n_{\Gamma, \mu}^{\sigma}(\epsilon)$ given by Figs. 4, 5, 6, and 9, we calculate Δm , given in Tables III and IV. We find local moments of $\Delta m = 1.42\mu_B$ in the SIC-LSD case and $\Delta m = 1.14\mu_B$ in the LSD case. Whereas the total magnetic moment ΔM is $2.0\mu_B$, much like in the d^8 free atom, the local magnetic moment Δm in the impurity orbital subspace is reduced and the remaining

$$\left[1 - \frac{1.42}{2.0} \times 100 = 29\% \right]$$

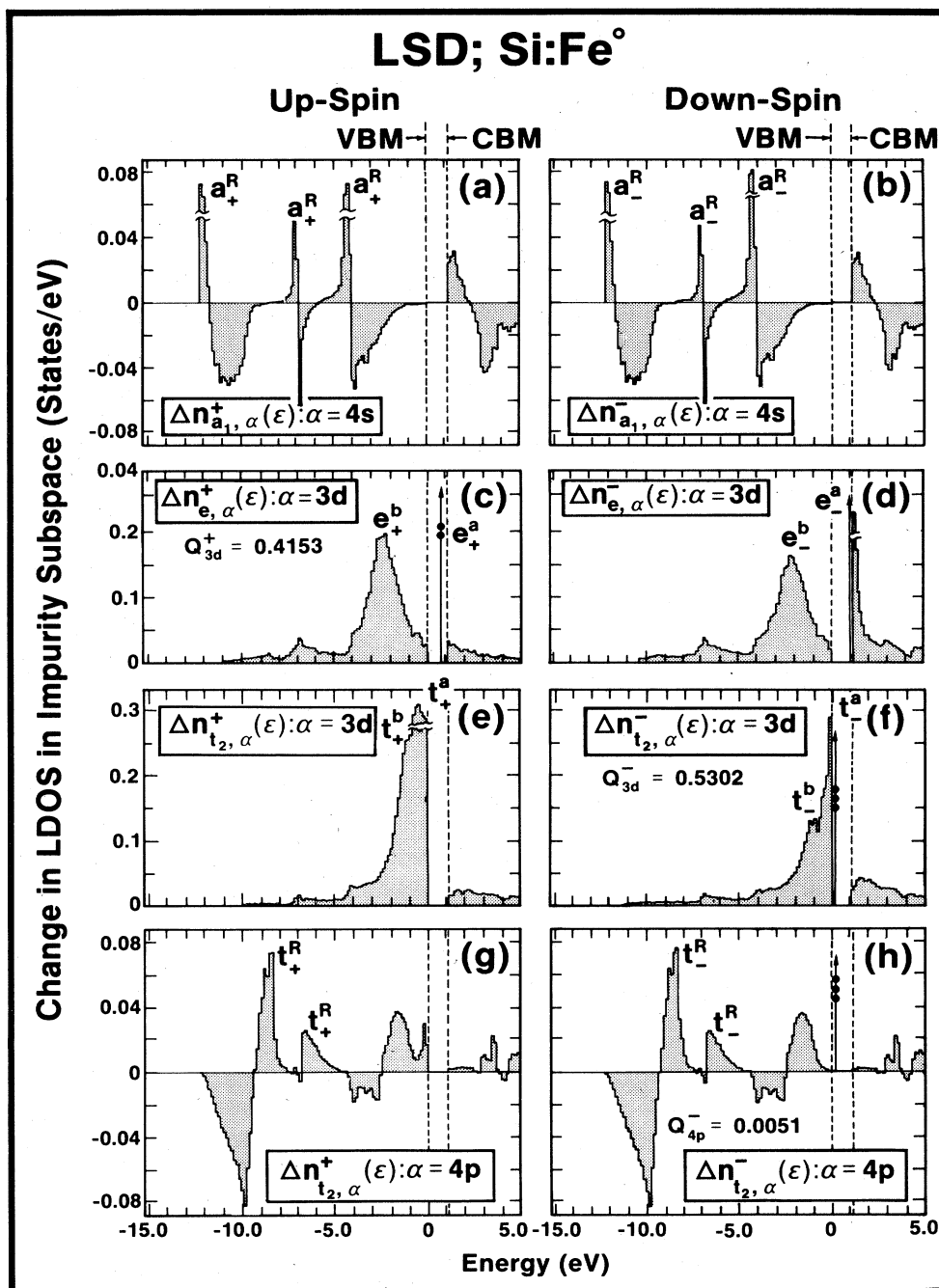


FIG. 9. Change $\Delta n_{\Gamma,\alpha}^{\sigma}(\epsilon)$ in the local density of states of Si:Fe⁰ in LSD for spin σ (+ or -) and the representation $\Gamma = a_1, e,$ and t_2 . We show only the major orbital components: $\alpha = 4s$ for a_1 , $3d$ for e , and $3d$ and $4p$ for t_2 .

of the magnetic moment is delocalized through the crystal, indicating substantial covalency. This local moment is reduced both relative to that of the bulk silicide^{58(a)} FeSi (1.94–2.38 μ_B), and to ferromagnetic iron (2.2 μ_B [Ref. 58(b)]). A population analysis of the local moment (Table III) shows it to evolve primarily from the valence d orbitals [distribution of local magnetic moments among the various orbitals

$$(\text{core})^{0.00}4s^{0.01}4p^{0.01}3d^{1.29}4d^{0.10}4f^{0.00}],$$

to be shared in a 5:1 proportion between the e and t_2 valence representations [distribution of local magnetic moments among the various representations of

$$(\text{core})^{0.00}a_1^{0.01}e^{1.17}t_2^{0.24}],$$

and to be dominated by the valence-band resonances ($\Delta m^{\text{VB}} = 1.61\mu_B$), with a smaller contribution from the gap states ($\Delta m^{\text{gap}} = -0.19\mu_B$). The significant difference between the Fe impurity in silicon as opposed to $3d$ im-

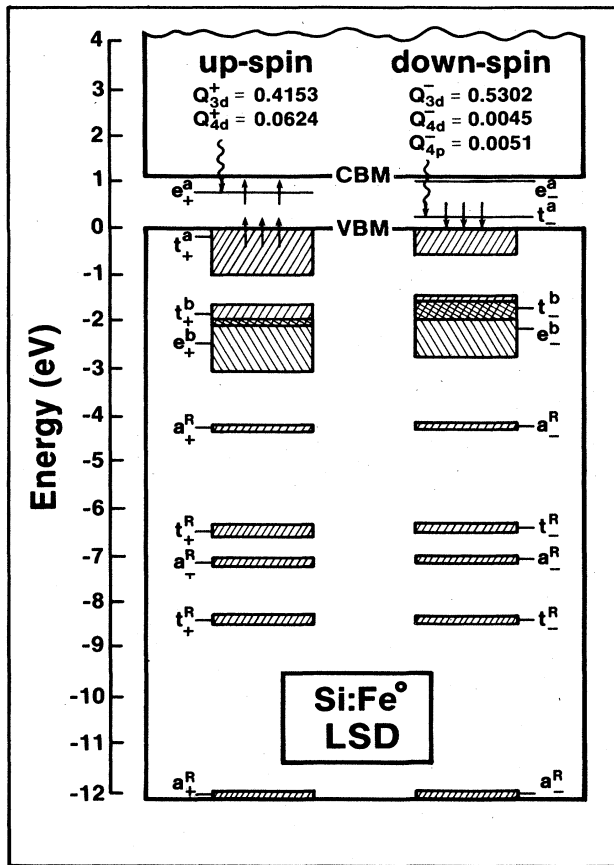


FIG. 10. Calculated impurity-induced levels and the width of the half value of the peak for Si:Fe^0 in LSD, showing the bonding (b), antibonding (a), resonance (R), up-spin ($+$), and down-spin ($-$) levels.

purities in ionic crystals²⁸ is that in the former case, most of the amplitude of the $3d$ spin orbitals exists as localized bonding resonances in the valence band, whereas in the latter case, the d orbitals are isolated as nonbonding states, appearing exclusively in the band gap.²⁸

Hence, we conclude that out of the 8 valence electrons of Fe, 0.276 (0.555) are delocalized away from the impurity site in SIC-LSD (LSD) calculations, respectively. Of the remaining 7.72 (7.44) iron valence electrons, 6.76

(6.43) form resonances in the valence band, and 0.96 (1.02) appear as gap states, in the SIC-LSD (LSD) calculation, respectively. Regarding the magnetism, we find that most of it evolves from the valence-band resonances: Out of the 6.76 (6.43) valence electrons, 5.15 (5.23) electrons reside in two-electron bonds, whereas the remaining 1.61 (1.20) are uncoupled from the electron pairs and contribute to the local magnetic moments. In addition, the 0.96 (1.02) electrons in the gap levels contribute an opposite term to the local moments, i.e., -0.19 (-0.06). This can be compared with the qualitatively similar Pauling-Zerner^{58(b)} population analysis of ferromagnetic iron: In their description 5.78 of the iron electrons form (spd) two-electron bonds, whereas the remaining 2.22 electrons are unpaired, contributing to the saturation moment.

E. Hyperfine field and spin density

Figures 11 and 12 show the spin density $\delta\rho(r)$ in the impurity orbital subspace in the LSD-SIC and LSD calculations. At the impurity nucleus site we find the negative spin polarization that originates from the negative net core polarization. On the other hand, in the bond region at $r=0.03-2.9$ a.u., we find a large positive spin polarization originates from the $3d$ polarization, whereas past $r \approx 2.9$ a.u., we find a small negative $\delta\rho(r)$ due to the extra localization of the up-spin d orbitals relative to the down-spin orbitals. The negative spin polarization at the impurity nucleus is caused by the repulsive intra-atomic Coulomb interaction between the core electrons and the unpaired $3d$ electrons.

In Table V, we show the contribution of each orbital to the Fermi contact hyperfine field $H_{\text{hf}}^{(i)}$ [i.e., Eq. (26)], both in SIC-LSD and in LSD. The main contribution to $H_{\text{hf}}^{(i)}$ comes from the negative core polarization of the filled core s orbitals; however, $H_{\text{hf}}^{(i)}$ is determined by the large cancellation between the negative contribution from $1s$ and $2s$ orbitals, and the positive contribution from $3s$ core and $4s$ orbital. In the SIC-LSD case, the contribution to the Fermi contact interaction (both direct and core polarization) from the core states is $-24.50-278.52 + 179.70 = -123.32$ kG for the $1s$, $2s$, and $3s$ states, respectively, and that from the $4s$ (a_1 -like) valence-band states is only $+8.18$ kG, yielding a total contact term of -115.14 kG.

The hyperfine field contributed by the electron orbital magnetic moment [Eq. (28)] is estimated from the experi-

TABLE II. Impurity occupation [Eq. (22)] and total magnetic moment [Eq. (20)] (in the whole space) for Si:Fe^0 , calculated both in SIC-LSD and LSD. We present separately the contributions due to occupied states in the valence band (VB, including all lower corelike states), as well as the contribution of the gap states alone.

	Impurity occupation (ΔZ)			Net Magnetization (ΔM)		
	VB	Gap	Total	VB (μ_B)	Gap (μ_B)	Total (μ_B)
Core	18.0	0.0	18.0	0.0	0.0	0.0
a_1	0.0	0.0	0.0	0.0	0.0	0.0
e	0.0	2.0	2.0	0.0	2.0	2.0
t_2	3.0	3.0	6.0	3.0	-3.0	0.0
(Sum)	21.0	5.0	26.0	3.0	-1.0	2.0

TABLE III. Impurity occupation [Eq. (25)] and the local magnetic moment [Eq. (23)] in the impurity orbital subspace of Si:Fe⁰ calculated in the SIC-LSD method.

	Impurity occupation			Net magnetization		
	VB	Gap	Total	VB (μ_B)	Gap (μ_B)	Total (μ_B)
Core	18.0	0.0	18.0	0.0	0.0	0.0
a_1	0.0577	0.0	0.0577	0.0121	0.0	0.0121
e	1.8064	0.3837	2.1901	0.7844	0.3837	1.1681
t_2	4.9000	0.5758	5.4758	0.8136	-0.5758	0.2378
(Sum)	24.7641	0.9595	25.7236	1.6101	-0.1921	1.4180
$4s$	0.0605	0.0	0.0605	0.0095	0.0	0.0095
$4p$	-0.1384	0.0072	-0.1312	0.0190	-0.0072	0.0118
$3d$	7.3217	0.8574	8.1791	1.5675	-0.2736	1.2939
$4d$	-0.4769	0.0949	-0.3820	0.0115	0.0887	0.1002
$4f$	-0.0028	0.0	-0.0028	0.0026	0.0	0.0026
(Sum)	24.7641	0.9595	25.7236	1.6101	-0.1921	1.4180
Q_{net}			0.2764			

TABLE IV. Impurity occupation [Eq. (25)] and the local magnetic moment [Eq. (23)] in the impurity orbital subspace of calculated Si:Fe⁰ in the LSD method.

	Impurity occupation			Net magnetization		
	VB	Gap	Total	VB (μ_B)	Gap (μ_B)	Total (μ_B)
Core	18.0	0.0	18.0	0.0	0.0	0.0
a_1	-0.1141	0.0	-0.1141	-0.0017	0.0	-0.0017
e	1.6483	0.4777	2.1260	0.6073	0.4777	1.0850
t_2	4.8931	0.5398	5.4329	0.5985	-0.5398	0.0587
(Sum)	24.4273	1.0175	25.4448	1.2041	-0.0621	1.1420
$4s$	-0.1128	0.0	-0.1128	-0.0022	0.0	-0.0022
$4p$	0.0722	0.0051	0.0773	0.0136	-0.0051	0.0085
$3d$	6.9614	0.9455	7.9064	1.1688	-0.1149	1.0539
$4d$	-0.4922	0.0669	-0.4253	0.0234	0.0579	0.0813
$4f$	-0.0013	0.0	-0.0013	0.0005	0.0	0.0005
(Sum)	24.4273	1.0175	25.4448	1.2041	-0.0621	1.1420
Q_{net}			0.5552			

mentally determined g shift ($\Delta g = +0.0676$ [Ref. 18(a)] or 0.0677 [Ref. 18(b)]) and the calculated value of $\langle 1/r^3 \rangle_{\text{av}}$ at $\epsilon = \epsilon_F$ (for SIC-LSD $\langle 1/r^3 \rangle_{\text{av}} = 0.5940$ a.u.⁻³, while for LSD $\langle 1/r^3 \rangle_{\text{av}} = 0.8150$ a.u.⁻³). We find this contribution to H_{hf} to be +5.02 kG in SIC-LSD, and to be +6.90 kG in LSD. Note that $H_{\text{hf}}^{(\text{ii})}$ is small and positive because the orbital magnetic moment is quenched ($L = 0$, $J = 1$, $S = 1$ in the case of Si:Fe⁰; t_2 states are ful-

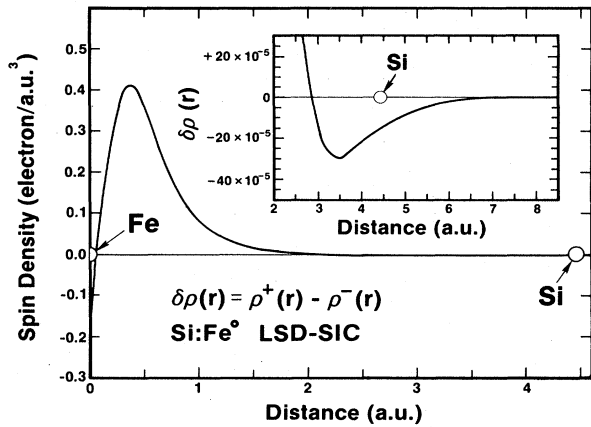
ly occupied). Neglecting the small dipolar term, the total calculated H_{hf} of -110.12 kG is reasonably close to the observed value of $|H_{\text{hf}}|$, 147.6 kG [Ref. 18(b)] or 152.2 kG [Ref. 18(a)]. We find a spin density at the Fe nucleus of $\delta\rho(0) = -0.220$ a.u.⁻³ in reasonable agreement with the observed values of $|\delta\rho(0)| = 0.282$ a.u.⁻³ [Ref. 18(b)] or 0.299 a.u.⁻³ [Ref. 18(a)]. Whereas only the absolute magnitude of $\delta\rho(0)$ and H_{hf} is available from experiment,¹⁸ our calculation shows both to be negative.

TABLE V. Comparison of different orbital contributions (in kG) to the contact hyperfine field in Si:Fe⁰.

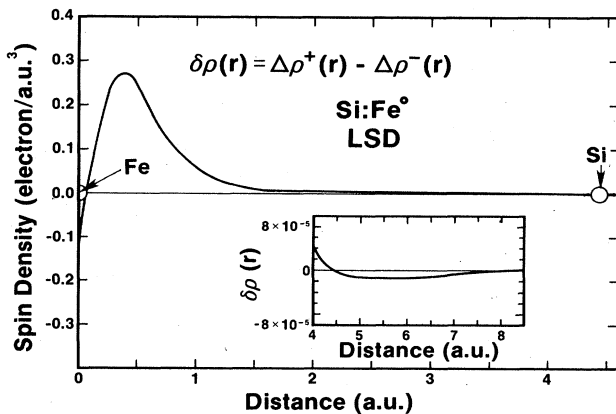
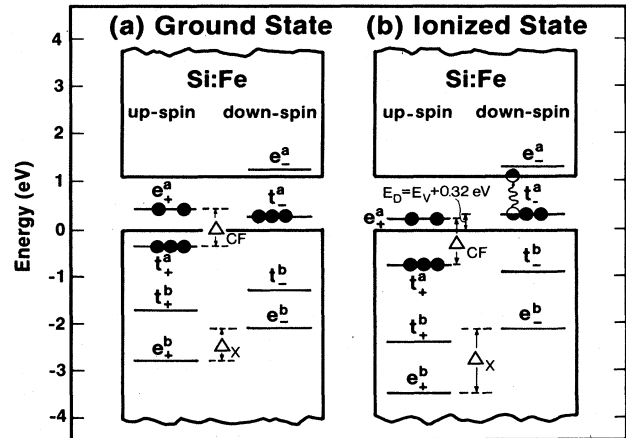
Orbital	LSD	SIC-LSD
1s	-19.61	-24.50
2s	-202.23	-278.52
3s	136.81	179.70
4s	5.21	8.18
Total	-79.82	-115.14

F. Doner ionization energy from Si:Fe⁰ to Si:Fe⁺ and the self-regulating response

To understand the apparent localized nature of Si:Fe⁺ with its attendant high-spin configuration,¹⁸ we performed calculations for this ionized state. Using Slater's transition-state approximation, we removed half an electron from either the e_+^a or the t_-^a gap levels [Fig. 13(a)], placing the ionized charge in the conduction-band minimum (CBM) and seeking a self-consistent solution.

FIG. 11. Calculated spin density for Si:Fe⁰ in SIC-LSD.

We find that although the highest occupied orbital of the neutral system is the e_+^a state [Fig. 13(a)], the lowest energy ionization process proceeds instead from the t_-^a orbital [Fig. 13(b)]. Remarkably, upon ionizing the t_-^a orbital, the e_+^a orbital moves down in energy, exposing the t_-^a as the highest occupied state of the ion and thereby producing the observed high-spin (weak-field) configuration and a donor energy $\epsilon(t_-^a) - \epsilon_{\text{VBM}} = E_v + 0.32$ eV, in good agreement with the observed value^{5,9,11-13} of $E_v = 0.385 \pm 0.01$ eV. Unlike the situation in the cluster calculation,⁵⁰ no stable acceptor state (Fe^0/Fe^-) is found in the gap, as the e_-^a level that would accommodate the next electron is in the conduction band [Fig. 13(a)]. This is consistent with the experiment.¹⁵ The reason for this $e_+^a - t_-^a$ level reversal is that upon ionizing a spin-down orbital, the highly localized (bonding) spin-up resonances in the valence band are relieved from their Coulomb repulsion with the ionized orbital and move to more negative energies. The valence-band resonance for down-spin orbital becomes less d -like and more hostlike upon ioniza-

FIG. 12. Calculated spin density for Si:Fe⁰ in LSD.FIG. 13. Calculated impurity-induced levels for (a) neutral Fe impurity, (b) positively charged Fe impurity, showing the bonding (b), antibonding (a), spin-up ($+$), and spin-down ($-$) levels in SIC-LSD.

tion. At the same time the d character of the gap states (t_-^a) increases substantially. The net effect is to keep the total impurity charge almost constant upon ionization, but this is mainly accomplished because the gap states (t_-^a) becomes much more d -like and localized rather than because of increased localization of the valence-band resonances for down-spin states. What appears to be happening is that the impurity d states for down-spin are being pushed up in energy upon ionization because of the increases of the spin polarization, thereby decreasing the impurity occupation of the down-spin valence-band resonances (making them more hostlike) and increasing the impurity content of the gap states. Becoming thus more localized, their spin polarization increases and the antibonding down-spin orbital t_-^a is now the highest occupied level. Hence, this ionization is accompanied by a switch of $\Delta_x/\Delta_{\text{CF}}$ from below unity for Si:Fe⁰ to above unity (1.4) for Si:Fe⁺, with the attendant formation of a high-spin state and an enhanced local magnetic moment of $\Delta m = 1.87\mu_B$ (Table VI). A population analysis of the magnetic moment (Table VI) shows a substantial increase in the t_2 contributions between the ground states and the ionized states [distribution of local moments in the different representations is

$$(\text{core})^{0.00} a_1^{0.01} e^{1.17} t_2^{0.24}$$

for Si:Fe⁰ versus

$$(\text{core})^{0.00} a_1^{0.02} e^{1.21} t_2^{0.64}$$

for Si:Fe^{+0.5}]. This change evolves primarily from the changed d orbital occupation [distribution of local moments from different orbitals is

$$(\text{core})^{0.00} 4s^{0.00} 4p^{0.01} 3d^{1.29} 4d^{0.10} 4f^{0.00}$$

for Si:Fe⁰ versus

$$(\text{core})^{0.00} 4s^{0.01} 4p^{0.00} 3d^{1.73} 4d^{0.11} 4f^{0.00}$$

TABLE VI. Impurity occupation [Eq. (25)] and the local magnetic moment [Eq. (23)] in the impurity orbital subspace of Si:Fe^{+0.5} in Slater's transition states.

	Impurity occupation			Net magnetization		
	VB	Gap	Total	VB (μ_B)	Gap (μ_B)	Total (μ_B)
Core	18.0	0.0	18.0	0.0	0.0	0.0
a_1	0.0489	0.0	0.0489	0.0163	0.0	0.0163
e	1.6286	0.5711	2.1997	0.6404	0.5711	1.2115
t_2	3.8183	1.5598	5.3781	2.1973	-1.5598	0.6375
(Sum)	23.4958	2.1309	25.6267	2.8540	-0.9887	1.8653
4s	0.0532	0.0	0.0532	0.0134	0.0	0.0134
4p	-0.1402	0.0188	-0.1214	0.0264	-0.0188	0.0076
3d	6.1647	1.8995	8.0642	2.9067	-1.1723	1.7344
4d	-0.5776	0.2126	-0.3650	-0.0954	0.2024	0.107
4f	-0.0043	0.0	-0.0043	0.0029	0.0	0.0029
(Sum)	23.4958	2.1309	25.6267	2.8540	-0.9887	1.8653
Q_{net}			0.3733			

for Si:Fe^{+0.5}]. This population analysis reveals that the change in the effective orbital configuration between the ground state and ionized state is small [effective electronic configuration of

$$(\text{core})^{18.0}4s^{0.06}4p^{-0.13}3d^{8.18}4d^{-0.38}4f^{-0.00}$$

for Si:Fe⁰ versus

$$(\text{core})^{18.0}4s^{0.05}4p^{-0.12}3d^{8.06}4d^{-0.37}4f^{-0.00}$$

for Si:Fe^{+0.5}]. Hence, the net impurity charge changes only slightly upon ionization: from $Q_{\text{net}}=0.276e$ to $Q_{\text{net}}=0.373e$ for Si:Fe^{+0.5} (i.e., for each ionized gap electron, only 0.195e is actually removed from the impurity orbital subspace, the remaining $1-0.195=0.805$ hole charge being distributed throughout the crystal). The reason for this self-regulating response^{41,59} is that the valence-band resonances become more localized upon removal of a gap electron, better penetrating the impurity site and making up for most of the charge removed by ionization. The effective Coulomb repulsion U^{dd} is, hence, very small^{41,59} [$U^{dd} \sim \frac{1}{2}(\Delta Q_{\text{net}})^2 U = 0.019U$, where U is the Coulomb repulsion of free ion]; and even an "overcrowded" d^8 configuration can be stable. This phenomenon is particular to $3d$ impurities in covalent media, where the existence of impurity resonances in the valence band provides a feedback interaction channel that does not exist in free atoms or in $3d$ impurities in ionic solids. In this latter case, ionized species can be stabilized by a massive relaxation of the crystal.⁶⁰ The self-regulating response has an obvious implication on the nature of the isomer shift. We discuss this point next.

G. Change of the Mössbauer isomer shift upon ionization

We find a surprisingly small calculated change in the isomer shift upon ionization, i.e., $\Delta_{\text{IS}}(\text{Si:Fe}^+) - \Delta_{\text{IS}}(\text{Si:Fe}^0) = -0.06$ mm/sec [using Eq. (29)]. This change is about 1 order of magnitude smaller than the change in the free atom upon an ionization, i.e., $\Delta_{\text{IS}}(\text{Fe}^{3+}) - \Delta_{\text{IS}}(\text{Fe}^{2+}) = -0.349$ mm/sec and $\Delta_{\text{IS}}(\text{Fe}^{4+}) - \Delta_{\text{IS}}(\text{Fe}^{3+}) = -0.569$ mm/sec, using Hartree-Fock values.⁶¹ The mechanism leading to the small change in

the isomer shift upon ionization in our model is simple: whereas Si:Fe⁰ has much of its charge density delocalized on the ligands, when converted to Si:Fe⁺, charge flows from the ligands to the impurity (through orbital relaxations), causing both Si:Fe⁰ and Si:Fe⁺ to have a comparable ionic charge at the impurity nucleus. We find indeed that the net impurity charge Q_{net} increases in the impurity orbital subspace only 0.195e upon ionization. This mechanism suggests that the charge density on the impurity site (as could be measured by the Mössbauer isomer shift) will change only a little by ionizing the impurity, whereas the largest change in density upon ionization would occur on the ligands. ENDOR experiments on the ionized impurity (i.e., in p -doped sample) could be used to examine this prediction. Unfortunately, while existing Mössbauer data^{24(a)} indeed show a vanishing change in the isomer shift of Si:Fe upon ionization, the data available to date are clouded by the occurrence of complexes.^{24(b)}

H. Comparison of SIC-LSD with LSD

In Table VII, we summarize the results of the SIC-LSD calculation with those obtained by the LSD calculation. The major effects due to SIC parallel the changes in atomic calculations discussed in Sec. III G. They are (i) a strong shift of all the occupied pure d (i.e., e representation) levels to more negative energies (e.g., the valence-band resonance e_+^b by 0.42 eV, and the gap level e_+^a by 0.33 eV), as they are relieved from the (repulsive) self-interaction; (ii) a corresponding upward shift of the occupied orbitals that contain substantial non- d character (e.g., the t_+^b and t_-^b valence-band resonances move up by 0.09 and 0.4 eV, respectively, whereas the t_+^a gap level moves up to 0.08 eV. This is a result of a feedback effect (non- d orbitals are now screened better by the $3d$ orbitals that became more localized), similar to that in free atoms ($4s$, $4p$ orbitals expand, $3d$ orbitals contract due to SIC); (iii) an upward shift of the unoccupied orbitals relative to the occupied orbitals (e.g., e_+^a moves up to 0.42 eV, penetrating the conduction band). The main consequences of these SIC-induced shifts are a strong enhancement of $\Delta_x/\Delta_{\text{CF}}$ (from 0.33 to 0.88), an increase in the local magnetic mo-

TABLE VII. Comparison of the SIC-LSD results with the results of the LSD calculation for Si:Fe⁰.

	SIC-LSD	LSD
Δ_x	0.70 eV	0.30 eV
Δ_{CF}	0.80 eV	0.90 eV
Δ_x/Δ_{CF}	0.88	0.33
Δm^{VB}	$1.61\mu_B$	$1.20\mu_B$
Δm^{gap}	$-0.19\mu_B$	$-0.06\mu_B$
Δm^{total}	$1.42\mu_B$	$1.14\mu_B$
$\epsilon(t_-^a)$	$E_v + 0.26$ eV	$E_v + 0.18$ eV
$\epsilon(e_+^a)$	$E_v + 0.44$ eV	$E_v + 0.76$ eV
$\epsilon(t_+^a)$	$E_v - 0.32$ eV	$E_v - 0.20$ eV
$\epsilon(e_-^a)$	$E_v + 1.21$ eV	$E_v + 1.01$ eV
$\epsilon(e_+^b)$	$E_v - 2.80$ eV	$E_v - 2.38$ eV
$\epsilon(t_+^b)$	$E_v - 1.90$ eV	$E_v - 1.81$ eV
$\epsilon(e_-^b)$	$E_v - 2.10$ eV	$E_v - 2.10$ eV
$\epsilon(t_-^b)$	$E_v - 1.27$ eV	$E_v - 1.67$ eV
$H_{hf}^{(i)}$	-115.14 kG	-79.82 kG
Q_{total}	25.7236	25.4448
Q_{net}	0.2764	0.5552

ment (from $1.14\mu_B$ to $1.42\mu_B$), a corresponding reduction of the contact hyperfine field $H_{hf}^{(i)}$ (from -79.82 to -115.14 kG) and an overall attraction of more electronic charge to the impurity site [0.31 more d electrons and 0.03 fewer non- d electrons, changing the *net* ionic impurity charge from $+0.555e$ (LSD) to $+0.276e$ (SIC-LSD)]. (iv) Since in LSD $\Delta_x/\Delta_{CF} < 1$, we do not obtain the experimentally observed high-spin ground state of Si:Fe⁺. We do obtain this high-spin ground state of Si:Fe⁺ ($S = \frac{3}{2}$, i.e., Hund's rule, high spin) using the SIC-LSD method, confirming thereby the result obtained previously in a non-self-consistent SIC-LSD calculation.^{33(a)}

Our results are in marked contradiction with the cluster calculation of DeLeo *et al.*⁵⁰ who obtained a universal high-spin configuration in their LSD calculation. It has been previously shown^{33(a)} that this is an artifact of using a discrete level structure attendant upon a small cluster and the neglect of the nonspherical potential components in the impurity cell. These approximations combine to artificially reduce the crystal-field splitting in their model, leaving the exchange as the only strong interaction, hence $\Delta_x \gg \Delta_{CF}$ in all cases. Instead, we find that Δ_x and Δ_{CF} are in general comparable in magnitude and that the balance between them depends both on the impurity in question and its charge state. Extensive LSD-SIC calculations for all $3d$ impurities in silicon in numerous charge states (to be reported later⁶²) show that Δ_x outweighs Δ_{CF} only for the impurities studied extensively by Ludwig and Woodbury (e.g., Fe⁺, Mn⁺, Cr⁺). Both at the low- Z end of the $3d$ series (V^0 , T_i^0 , V^+) and at the high- Z end (Co and Ni), for which no data exist as yet, we predict a low-spin ground state. We conclude that whereas simplified LSD calculations can give a universal high-spin ground state, as originally argued by Ludwig and Woodbury to be

the case, more careful LSD-SIC calculations are needed to correctly establish the theoretical ground-state symmetry.

V. DISCUSSION

A. Duality in the nature of the localization

Based upon the calculated results, we will discuss the resolution to the apparent dichotomy between the covalently delocalized model and the atomically localized model for Si:Fe that has been posed in Sec. II. We first summarize the results for Si:Fe⁰, consistent with the CDM. For Si:Fe⁰, we find that (i) in contrast to the dominant role of the valence-band states in determining the local magnetic moment, the hyperfine field H_{hf} and the net spin density at the nucleus $\delta\rho(0)$ determined largely by the core states. Both calculated results are in good agreement with experiment and suggest reduction by covalent hybridization. (ii) The crystal-field splitting exceeds the exchange splitting ($\Delta_x/\Delta_{CF}=0.88$); hence, the t_-^a gap level is below the e_+^a level, which is the highest occupied state. This level arrangement is characteristic of a strong-field (covalent) situation^{18(a)} and correctly produces^{18(a)} (as also does the weak-field model) $S=1$. (iii) The s electrons are largely transferred into d orbitals ($s \rightarrow d$ promotion), which agrees with Ludwig and Woodbury.^{18(a)} This $s \rightarrow d$ population inversion decreases the effective size of the atom without converting it into an ion. This is the simple chemical reason for its high diffusivity and low solubility.⁵ Our results for Si:Fe⁰ are thus consistent with the covalently delocalized model.

Si:Fe⁺ has different characteristics. We find that (i) although the highest occupied orbital of the neutral system is the e_+^a state, the lowest energy ionization proceeds instead from the t_-^a orbital. Remarkably, upon ionizing t_-^a , the e_+^a orbital moves down in energy, exposing that t_-^a as the highest occupied state of the ion, thereby producing the observed $S = \frac{3}{2}$ high-spin (weak-field) configuration as Δ_x/Δ_{CF} switches from below unity for Si:Fe⁰ to above unity (1.4) for Si:Fe⁺. (ii) We find a donor energy $E(0/+)=E_v+0.32$ eV, in good agreement with the observed value^{12,15} of $E_v+0.385 \pm 0.01$ eV. (iii) In agreement with experiment,¹⁵ no stable acceptor state (Fe⁰/Fe⁻) exists in the gap, as the empty e_-^a level that would accommodate the next electron is in the conduction band (i.e., Fig. 13). (iv) The net impurity charge Q_{net} increases in the impurity orbital subspace only by $0.1e$ upon ionization. This self-regulating response^{41,59} of the valence band to excitations of the "outer" gap electrons means that the effective Coulomb repulsion U^{dd} is substantially smaller than what a linear dielectric screening mechanism would grant us, and even an "overcrowded" d^8 configuration can be stabilized. (v) We predict a vanishingly small change of the isomer shift upon ionization, i.e., $\Delta_{IS}(\text{Si:Fe}^+) - \Delta_{IS}(\text{Si:Fe}^0) \simeq -0.06$ mm/sec (about 1 order of magnitude smaller than the change in free atoms). The results for Si:Fe⁺ [(i) and (iii)] are hence consistent with the atomically localized model and the others for Si:Fe⁺ [(ii), (iv), and (v)] are consistent with the covalently delocalized model. In addition, our results for Si:Fe⁰ clearly show that most of the spin density ($\sim 71\%$)

is concentrated on the impurity cell (in agreement with recent ENDOR measurements²¹), supporting the ALM. Clearly, the electron density is considerably more extended than the spin density.

The resolution to the apparent dichotomy between the covalently delocalized and atomically localized models for Si:Fe lies therefore in this self-regulating response and in the fact that different orbitals are responsible for the different aspects of the localization (duality, not dichotomy): the contact spin density and hyperfine field are decided by the hyperlocalized core states, the magnetism is largely contributed by the localized valence-band resonances, and the donor ionization, with its attendant high-spin configuration, and the constancy of the Mössbauer isomer shift are decided by a combination of delocalized gap states and the feedback (self-regulating) response of the valence-band resonances to excitations of the outer states.

B. Covalent reduction of the hyperfine field

Compared with the hyperfine field $H_{\text{hf}} = -350$ kG and the contact spin density $\delta\rho(0) = -0.668$ a.u.⁻³ of the free Fe atom (d^8) calculated in the Hartree-Fock approximation,²⁰ the EPR data¹⁸ for Si:Fe yielding $|H_{\text{hf}}| = 147.6$ or 152.2 kG and $|\delta\rho(0)| = 0.282$ or 0.299 a.u.⁻³ shows a substantial reduction ($\sim 43\%$) in the hyperfine field and the spin density. Recall that the contact hyperfine field originates from⁹ mismatch between spin-up and spin-down densities of the hyperlocalized s orbitals of the impurity, and that this mismatch is induced solely through the polarization of these core states by the outer $3d$ electrons which carry the magnetism.⁴² The intra-atomic Coulomb repulsion U_{sd} hence controls the contact hyperfine field. The reduction in this field H_{hf} relative to the free atom results from covalent hybridization of the outer $3d$ orbitals: Since about 30% of the $3d$ character is found to be delocalized through the crystal due to this hybridization, the intra-atomic repulsion U_{sd} with the localized core electrons is diminished, leading to a smaller H_{hf} at the nucleus. The correlation of H_{hf} with covalency is further illustrated in Fig. 14 which shows the experimentally observed²⁶ hyperfine field of Fe impurity nuclei per electron spin S in various systems. The horizontal axis depicts covalency evaluated from the electronegativity of Gordy and Thomas⁶³ using empirical equations.^{26,64} From these results, we can conclude that the absolute value of the hyperfine field decreases with increasing covalency. The hyperfine field H_{hf} of the Fe impurity in an ionic crystal (e.g., Fe in CaCO_3 , MgO , CaO , Al_2O_3 in Fig. 14) is very close to the H_{hf} of the free atom obtained in the Hartree-Fock calculation.²⁰ In contrast, in the case of a covalent semiconductor, as the covalent hybridization is stronger, the impurity wave function becomes more extended than in the ionic crystals. Hence, we observe a reduction in the spin density $\delta\rho(0)$ and H_{hf} in Si:Fe.

We suspect that the reason of the very small g shift [$\Delta g \equiv g - (2.0023) = +0.0677$ to $+0.0676$ (Ref. 18) for Si:Fe⁰] also results from a covalent reduction in the spin-orbit coupling constant λ . Using the second-order perturbation theory, Δg is given by $\Delta g = -8k\lambda_0/\Delta_{\text{CF}}$, where λ_0 is the spin-orbit coupling constant of free atom (Fe⁰, d^8),

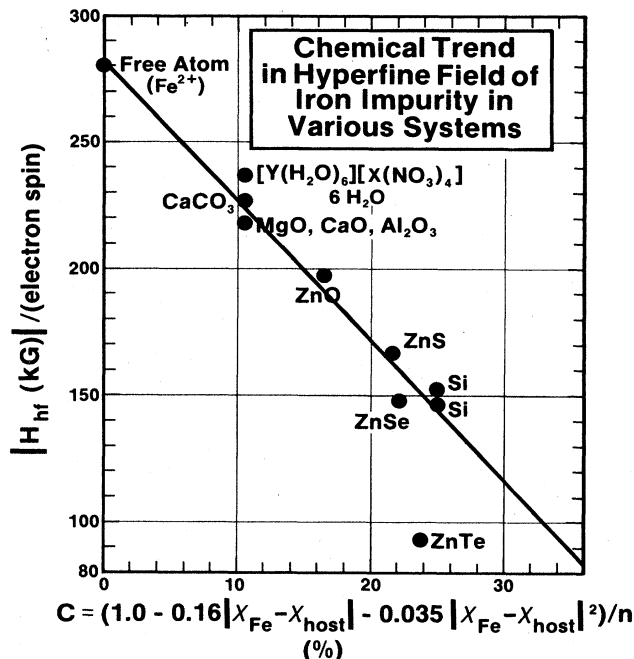


FIG. 14. Chemical trend in H_{hf} of Fe impurity in various systems per electron spin S . C is the covalency (%) given by $C = (1.0 - 0.16|\chi_{\text{Fe}} - \chi_{\text{host}}| - 0.035|\chi_{\text{Fe}} - \chi_{\text{host}}|^2)/n$, where χ_{Fe} and χ_{host} are the electronegativity of Fe and the nearest-neighbor host atom, and n is the number of the coordination around the Fe impurity.

k is the reduction ratio of the spin-orbit coupling constant defined by $k \equiv \lambda/\lambda_0$; and Δ_{CF} is the crystal-field splitting between t_2 and e states. We use $\lambda_0 = -112$ cm⁻¹ from the free atom and $\Delta_{\text{CF}} = 0.80$ eV from the present calculation (Table VII). We can estimate k from the ratio between $\langle r^{-3} \rangle_{\text{av}}$ for Si:Fe⁰ and for Fe⁰(d^8). From the calculated value of $\langle r^{-3} \rangle_{\text{av}}$ for Si:Fe⁰ (0.6150 at $\epsilon = \epsilon(t_a^-)$ a.u.⁻³) and that for⁴² Fe⁰(d^8) (3.8822 a.u.⁻³) we obtain $k = 0.1584$. Therefore, we obtain $\Delta g = +0.0220$. This compares well with the experimentally observed value of $\Delta g = +0.0677$ or $+0.0676$.¹⁸ Hence, a small value of k is consistent with covalent reduction.

C. Speculation on the redox ionization energy in heme proteins and cytochrome-C

The origin of the stability of an overcrowded d^8 configuration of Si:Fe is the self-regulating response^{41,59} caused by the covalency and nonlinear screening. If one refers the experimental donor ionization energy of Si:Fe⁰ to a vacuum, one finds the d^8 electrons to be bound by as much as $\sim 4.8 \pm 0.2$ eV. This value is characteristic of the far more stable doubly-ionized Fe²⁺ impurity in heme proteins and in electron-transporting biological systems (e.g., 5.0–5.3 eV for an ionization energy of Fe²⁺ in a polar electrolyte³² or for the strongly bonded iron in⁶⁵ cytochrome-C). We suspect that a similar self-regulating (Le Chatelier) response is the reason why Fe²⁺/Fe³⁺ redox ionizations in heme proteins and electron-transporting biological systems take so little energy,⁶⁵

despite the fact that the molecule is not severely distorted. The electronic structures of heme proteins and cytochrome-*C* have several similarities to that of the iron impurity in a semiconductor: (i) The free-electron-like π orbitals in the porphyrin ring show a small band gap between the bonding and antibonding states,⁶⁶ (ii) the iron $3d$ orbitals hybridize strongly with the π electrons in the porphyrin ring, and (iii) an integer number of spins is observed in the measurement of the magnetization in the heme protein,⁶⁷ suggesting a discrete bound state in the band gap. We, hence, suspect that the small redox energies involved in these systems result from the same self-regulating response,^{41,59} which is available to the $3d$ impurity in covalent semiconductors.

D. Comparison with other calculations

Hoshino and Suzuki⁶⁸ calculated the spin-restricted electronic structure and the donor ionization energy of Si:Fe⁰ using a small cluster (FeSi₁₀) embedded in a Bethe lattice. They found that (i) a_1 , t_2 , and e bound states exist in the band gap, in the order $\epsilon(a_1) < \epsilon(e) < \epsilon(t_2)$; (ii) the electron configuration of the ground states is $d^{7.06}_s 0.88$ and $a_1^1 e^4 t_2^3$; (iii) they identify the donor ionization energy with the excitation of an electron from an a_1 gap state to the conduction band (rather than from the t_2 state), as they argue that the e and t_2 bound states are so strongly localized on the impurity that no ionization could occur at low energy. These results are in substantial disagreement with our calculation and the results from nonmagnetic calculations of the QBCF method.³³ The crystal-field splitting is too small ($\Delta_{CF} \sim 0.04$ eV) compared with our calculation ($\Delta_{CF} = 0.8$ eV) and QBCF ($\Delta_{CF} = 0.6$ eV), and the energy of t_2 bound states is higher than e states. This is the opposite of our calculation, the QBCF calculation,³³ and the Ludwig and Woodbury phenomenological model.^{18(a)} Also, we did not find any a_1 bound states in the gap. Note that our self-consistent calculation shows that even localized states could have a low-energy donor transition due to the self-regulating effect.

Recently, DeLeo *et al.*⁵⁰ calculated the spin-polarized electronic structure of the $3d$ impurity in silicon using a small cluster (Si₁₀H₁₆:Fe) in a multiple-scattering $X\alpha$ cluster (MS $X\alpha$ cluster) method. They obtained (i) the donor ionization energy of Si:Fe⁰ in the case of magnetic states to be $E(0/+)=E_v+0.53$ eV, and a stable Fe acceptor level (for which there is no experimental evidence¹⁵), (ii) a vanishingly small crystal-field splitting ($\Delta_{CF} \sim 0.025$ eV), (iii) a very large exchange splitting Δ_x for Si:Fe⁰ (~ 1 eV), with the t_- level above the e_+ level, and (iv) sharp valence-band resonances. This situation resembles a highly localized, atomiclike impurity in the ionic crystal, where $\Delta_x/\Delta_{CF} \gg 1$. It was subsequently shown^{33(a)} that this atomiclike picture results both from their spherical approximation and from the limited availability of host states capable of hybridizing with Fe in their small cluster model (discussed in Sec. IVA). This underestimates covalent interactions in favor of atomic localization. In accordance with this analysis we obtain in our (non-SIC) LSD calculations very different results: $\Delta_x = 0.3$ eV $<$ Δ_{CF} , no acceptor state, a lower donor state

at $E_v+0.32$ eV, a t_- level below the e_+ level, and very broad resonances.

Recently, Pecheur and Toussaint⁶⁹ (PT) have performed charge self-consistent tight-binding calculations on a number of $3d$ impurities in Si. In general, they find considerably larger crystal-field splittings than in the MS $X\alpha$ cluster calculation of DeLeo *et al.*⁵⁰ PT characterize their results as corresponding to a picture of partially delocalized $3d$ orbitals, contrasted with the atomically localized $3d$ orbitals evident in the cluster calculation. Both conclusions agree with the present results. However, significant differences remain between the tight-binding results for Si:Fe and the present results: The energy levels in the latter calculation seem to be lowered substantially relative to ours. For example, for Si:Fe⁰ they find the e_-^a and t_-^a levels at $E_v+0.36$ eV and $E_v-0.06$ eV, respectively, whereas in the present SIC-LSD calculation we find them at $E_v+1.3$ eV and $E_v+0.26$ eV, respectively (Table VII). They find no e_+^a state in the gap, whereas our e_+^a level appears at $E_v+0.44$ eV. Since their donor orbital t_-^a is inside the valence band for the neutral center (where t_-^a has three electrons), when ionized, they find it to still be inside the valence band, hence they predict a negative donor energy (unobservable), while we find it at $E_v+0.32$ eV.

The results of the present study are similar to the spin-unpolarized QBCF local-spin-density results of Zunger and Lindefelt.³³ Taking the spin-occupation average of the e_+^a and e_-^a gap level energies we find here $E_v+0.76$ eV, compared with the QBCF results of $E_v+0.8$ eV. The comparison with the t_2^a levels is complicated somewhat by the fact that t_+^a is a broad resonance and not a sharp gap level like e_\pm^a . The weighted average of the present calculation gives $E_v-0.01 \pm 0.4$ eV compared with the QBCF results of $E_v+0.12$ eV. The population analysis also produces similar results, as discussed above. The use of the method of Williams *et al.*³⁶ for obtaining an augmented Green's function produces essentially the same results as the use of the quasiband method.³⁵

VI. SUMMARY

The spin-polarized electronic structure of an interstitial iron impurity in silicon was calculated self-consistently using the self-interaction-corrected local-spin-density functional formalism. The salient features of our results follow.

(i) The self-interaction correction is necessary to obtain the correct high-spin ground state of Si:Fe⁺, in agreement with our previous perturbative calculation^{33(a)} but in disagreement with the results of the cluster model.⁵⁰ Relative to the LSD it also changes the hyperfine field by 30%, bringing it close to experimental values reduces substantially the ionicity of the system, and increases the local magnetic moment by 20%.

(ii) We find a ground-state configuration $t_-^3 e_+^2$ for Si:Fe⁰ and $t_-^2 e_+^2$ for Si:Fe⁺. The donor energy corresponding to the transition between these states is calculated to be $E_v+0.32$ eV, in good agreement with experiment ($E_v+0.385$ eV). No stable acceptor state is found in the gap. Strong valence-band resonances are found which control the donor ionization energy through their orbital

relaxation attendant upon ionizing the outer gap levels.

(iii) The calculated central hyperfine field of -110.12 kG is comparable to the observed value of 147.6 or 152.2 kG. We find most of the contact contribution to the hyperfine field to evolve from the polarized core orbitals, largely through a balance between the large negative $1s + 2s$ contribution (-303 kG) and the positive $3s + 4s$ contribution (187.9 kG).

(iv) Whereas the total magnetic moment of Si:Fe^0 is $2.0\mu_B$, the local moment is only $1.42\mu_B$, suggesting some delocalization of the net spin density through the crystal. Out of the 26 electrons of Fe^0 , $0.276e$ are effectively transferred to the ligands, suggesting only a small role of ionicity. Of the remaining 25.724 electrons, 18 are in core orbitals and 7.72 are in valence states. Of these, $6.76e$ form valence-band resonances and $0.96e$ reside in gap levels. Most of the magnetism evolves from the valence-band resonances: They give rise to a moment of $1.61\mu_B$, whereas the gap electrons contribute a negative moment of $-0.19\mu_B$. The distribution of the local magnetic moment among the different orbitals is

$$(\text{core})^{0.0}4s^{0.01}4p^{0.01}3d^{1.29}4d^{0.10}4f^{0.00}$$

(i.e., essentially localized on $3d$), whereas the distribution among the representations is

$$(\text{core})^{0.0}a_1^{0.01}e^{1.17}t_2^{0.24}$$

(i.e., a 5:1 ratio between e and t_2 contributions). The effective orbital configuration of Si:Fe^0 shows that almost all of the $4s$ electrons have moved into the $3d$ shell.

(v) While $3d$ impurities in ionic host crystals have their levels concentrated inside the band gap, with little coupling to the host bands, in silicon, the existence of massive

valence-band resonances is indicative of substantial coupling and controls the local magnetic moment, orbital occupations, and optical properties. Hence, whereas the neutral center has some of its charge delocalized on the ligands, when ionized, the ligand orbitals relax, returning thereby to the impurity site much of the charge lost upon its ionization. Consequently, the *effective* charge on the impurity depends only weakly on its formal oxidation state. This suggests a small change in the Mössbauer isomer shift upon doping and leads to a remarkable reduction in the effective Coulomb repulsion U . This "self-regulating response" of the valence-band states to perturbations in the gap levels might very well be also the reason why it takes so little energy to perform the $\text{Fe}^{2+}/\text{Fe}^{3+}$ redox reaction in iron-containing biological molecules (e.g., cytochrome-C).

Note added in proof. We were recently informed [P. W. Anderson (private communication) for which we are grateful] that P. W. Anderson and D. Haldane have suggested earlier (unpublished results, 1976) the relevance of the self-regulating response (discussed here and in Refs. 40, 41, and 59) to biological Fe-containing systems.

ACKNOWLEDGMENTS

The authors are grateful to C. A. J. Ammerlaan, E. R. Weber, and J. M. Spaeth, for valuable correspondence and discussion concerning their experimental ENDOR data and to G. D. Watkins for helpful discussions. One of the authors (H.K.-Y.) also acknowledges K. Shindo and H. Akai for valuable discussions. This work was supported by the Office of Energy Research, Materials Science Division, U.S. Department of Energy, under Grant No. DE-AC02-77CH00178.

*Permanent address: Department of Physics, Tohoku University, Sendai 980, Japan.

¹E. R. Weber and H. G. Rietze, *J. Appl. Phys.* **51**, 1484 (1980).

²Y. H. Lee, R. L. Kleinhenz, and J. W. Corbett, *J. Appl. Phys. Lett.* **31**, 142 (1977).

³J. D. Struthers, *J. Appl. Phys.* **27**, 1560 (1956).

⁴L. C. Kimerling, in *Defects in Semiconductors*, edited by J. Narayan and T. Y. Tan (North-Holland, New York, 1981), p. 85.

⁵E. R. Weber, *J. Appl. Phys.* **30A**, 1 (1983).

⁶C. B. Collins and R. O. Carlson, *Phys. Rev.* **108**, 1409 (1957).

⁷R. H. Hopkins, R. G. Seidensticker, J. R. Davies, P. Rai-Choudhury, P. D. Blais, and J. R. McCormick, *J. Cryst. Growth* **42**, 493 (1977); A. Rohatgi, J. R. Davies, R. H. Hopkins, P. Rai-Choudhury, P. G. McMullin, and J. R. McCormick, *Solid State Electron.* **23**, 415 (1980).

⁸J. D. Gerson, L. J. Cheng, and J. W. Corbett, *J. Appl. Phys.* **48**, 4821 (1977).

⁹K. Graff and H. Pieper, *J. Electrochem. Soc.* **128**, 669 (1981).

¹⁰L. C. Kimerling, J. L. Benton, and J. J. Rubin, in *Defects and Radiation Effects in Semiconductors*, edited by R. R. Hasiguti (I.O.P., Bristol, 1981), p. 217.

¹¹H. Feichtinger, J. Waltl, and A. Gschwandtner, *Solid State Commun.* **27**, 867 (1978).

¹²K. Wüstel and P. Wagner, *J. Appl. Phys.* **A27**, 207 (1982).

¹³H. Lemke, *Phys. Status Solidi* **64A**, 215 (1981).

¹⁴K. Graff and H. Pieper, in *Semiconducting Silicon*, edited by

H. R. Huff, R. J. Kriegler, and Y. Takeishi (Electrochemical Society, Pennington, 1981), p. 331.

¹⁵H. Feichtinger and R. Czaputa, *Phys. Status Solidi* **79**, K143 (1983).

¹⁶S. H. Müller, G. M. Tuynman, E. G. Sieverts, and C. A. J. Ammerlaan, *Phys. Rev. B* **25**, 25 (1981).

¹⁷G. W. Ludwig, H. H. Woodbury, and R. O. Carlson, *Phys. Rev. Lett.* **1**, 295 (1958).

^{18(a)}G. W. Ludwig and H. H. Woodbury, *Solid State Phys.* **13**, 223 (1962); (b) E. G. Sieverts, S. H. Müller, C. A. J. Ammerlaan, and E. R. Weber, *Solid State Commun.* **47**, 631 (1983).

¹⁹The hyperfine coupling constant A is given by (Ref. 18) $A = (8\pi/3)g\mu_B g_N \beta_N |\phi(0)|_{\text{eff}}^2$, where g is the electron g factor, μ_B is the electron Bohr magneton, g_N is the nuclear g factor, β_N is the nuclear Bohr magneton, and $|\phi(0)|_{\text{eff}}^2$ is the *effective* electron spin density at the impurity nucleus, *per unpaired electron*. The corresponding hyperfine field H_{hf} is given by $H_{\text{hf}} = AS/g_N \beta_N$, where S is the total electron spin. The spin density at the impurity nucleus $\delta\rho(0)$ can be expressed as $\delta\rho(0) = 2S |\phi(0)|_{\text{eff}}^2$, if most of the hyperfine field comes from the Fermi contact interaction.

²⁰A. J. Freeman and R. E. Watson, *Phys. Rev. Lett.* **5**, 498 (1960).

²¹S. Greulich-Weber, J. R. Niklas, E. R. Weber, and J. M. Spaeth, *Phys. Rev. B* **30**, 6292 (1984).

²²F. S. Ham, *Phys. Rev.* **138**, A1727 (1965).

²³U. Lindelfelt and A. Zunger, *Phys. Rev. B* **30**, 1102 (1984).

- ²⁴(a) P. C. Norem and G. K. Wertheim, *J. Phys. Chem. Solids* **23**, 1111 (1962); (b) G. Weyer, A. Kettschau, G. Grebe, W. Schröter, and W. Bergholz, *Phys. Status Solidi A* **51**, 459 (1979).
- ²⁵R. Ingalls, F. Van der Woude, and G. A. Sawatzky, in *Mössbauer Isomer Shifts*, edited by G. K. Shenoy and F. E. Wagner (North-Holland, Amsterdam, 1978), p. 361; L. R. Walker, G. K. Wertheim, and V. Jaccarino, *Phys. Rev. Lett.* **6**, 98 (1961).
- ²⁶J. C. M. Henning, *Phys. Lett.* **24A**, 40 (1967).
- ²⁷C. E. Moore, *Atomic Energy Levels*, Natl. Bur. Stand. (U.S.) Spec. Publ. (No. 35/V.II, U.S. GPO, Washington, D.C., 1971), p. 49.
- ²⁸D. B. Chase and D. S. McClure, *J. Chem. Phys.* **64**, 74 (1976); J. G. Harrison, C. C. Lin, and W. Y. Ching, *Phys. Rev. B* **24**, 6060 (1981).
- ²⁹G. W. Gobeli and F. G. Allen, *Phys. Rev.* **127**, 141 (1962).
- ³⁰A. Fazzio, M. Caldas, and A. Zunger, *Phys. Rev. B* **29**, 5999 (1984); **30**, 3430 (1984).
- ³¹M. Caldas, A. Fazzio, and A. Zunger, *Appl. Phys. Lett.* **45**, 671 (1984).
- ³²K. E. Heusler, in *Encyclopedia of Electrochemistry of the Elements*, edited by A. J. Bard (Marcel Dekker, New York, 1982), p. 229.
- ³³(a) A. Zunger, *Phys. Rev. B* **28**, 3628 (1983); (b) A. Zunger and U. Lindefelt, *Phys. Rev. B* **26**, 5989 (1982); (c) U. Lindefelt and A. Zunger, *J. Phys. C* **17**, 6047 (1984).
- ³⁴H. Katayama-Yoshida and K. Shindo, *Phys. Rev. Lett.* **51**, 207 (1983); *J. Phys. Soc. Jpn.* **53**, 1114 (1984); *Solid State Commun.* **44**, 989 (1982).
- ³⁵U. Lindefelt and A. Zunger, *Phys. Rev. B* **26**, 846 (1982).
- ³⁶A. R. Williams, P. J. Feibelman, and N. D. Lang, *Phys. Rev. B* **26**, 5433 (1982).
- ³⁷D. J. Chadi, *Phys. Rev. B* **16**, 3572 (1977).
- ³⁸M. L. Cohen and T. K. Bergstresser, *Phys. Rev.* **141**, 789 (1966).
- ³⁹T. L. Loucks, *Augmented Plane Wave Method* (Benjamin, New York, 1967).
- ⁴⁰V. A. Singh and A. Zunger, *Phys. Rev. B* **31**, 3729 (1985).
- ⁴¹A. Zunger and U. Lindefelt, *Phys. Rev. B* **27**, 1191 (1983); *Solid State Commun.* **45**, 343 (1983); A. Zunger, *Phys. Rev. Lett.* **50**, 1215 (1983); V. Singh, U. Lindefelt, and A. Zunger, *Phys. Rev. B* **27**, 4909 (1983); **27**, 1420 (1983).
- ⁴²A. J. Freeman and R. E. Watson, in *Magnetism*, edited by G. Rado and H. Suhl (Academic, New York, 1965), p. 167.
- ⁴³C. P. Slichter, *Principles of Magnetic Resonance* (Harper and Row, New York, 1963).
- ⁴⁴S. Geschwind, in *Hyperfine Interactions*, edited by A. J. Freeman and R. B. Frankel (Academic, New York, 1967), p. 225.
- ⁴⁵B. D. Dunlap and G. M. Kalvius, in *Mössbauer Isomer Shifts*, edited by G. K. Shenoy and F. E. Wagner (North-Holland, Amsterdam, 1978), p. 15.
- ⁴⁶G. K. Shenoy and B. D. Dunlap, in *Mössbauer Isomer Shifts*, edited by G. K. Shenoy and F. E. Wagner (North-Holland, Amsterdam, 1978), p. 869.
- ⁴⁷H. Katayama-Yoshida and K. Shindo, *J. Magn. Magn. Mater.* **31-34**, 553 (1983).
- ⁴⁸A. Fazzio and J. R. Leite, *Phys. Rev. B* **21**, 4710 (1980).
- ⁴⁹L. A. Hemstreet, *Phys. Rev. B* **15**, 834 (1977); L. A. Hemstreet and J. P. Dimmock, *ibid.* **20**, 1527 (1979).
- ⁵⁰(a) G. G. DeLeo, G. D. Watkins, and W. B. Fowler, *Phys. Rev. B* **23**, 1851 (1981); (b) **25**, 4962 (1982); **25**, 4972 (1982).
- ⁵¹N. Gemma, *J. Phys. C* **17**, 2333 (1984).
- ⁵²W. Kohn and L. J. Sham, *Phys. Rev.* **140A**, 1133 (1965); O. Gunnarsson, B. I. Lundquist, and J. W. Wilkins, *Phys. Rev. B* **10**, 1319 (1974).
- ⁵³J. P. Perdew and A. Zunger, *Phys. Rev. B* **23**, 5048 (1981).
- ⁵⁴M. R. Pederson, R. A. Heaton, and C. C. Lin, *J. Chem. Phys.* **80**, 1972 (1984).
- ⁵⁵M. R. Norman, *Phys. Rev. B* **24**, 2456 (1984); R. A. Heaton and C. C. Lin, *J. Phys. C* **17**, 1853 (1984).
- ⁵⁶A. Zunger, J. P. Perdew, and G. L. Oliver, *Solid State Commun.* **34**, 933 (1980).
- ⁵⁷P. Bendt and A. Zunger, *Phys. Rev. B* **26**, 3114 (1982).
- ⁵⁸(a) F. Dupre, G. Frollani, F. Menzinger, and F. Sacchetti, *J. Phys. F* **9**, 691 (1979); (b) L. Pauling, *Proc. R. Soc. London, Ser. A* **378**, 207 (1981).
- ⁵⁹F. D. M. Haldane and P. W. Anderson, *Phys. Rev. B* **13**, 2553 (1976).
- ⁶⁰A. M. Stoneham and M. J. L. Sangster, *Philos. Mag.* **B43**, 609 (1981).
- ⁶¹A. J. Freeman and D. E. Ellis, in *Mössbauer Isomer Shifts*, edited by G. K. Shenoy and F. E. Wagner (North-Holland, Amsterdam, 1978), p. 111.
- ⁶²H. Katayama-Yoshida and A. Zunger, *Phys. Rev. Lett.* **53**, 1256 (1984); *Phys. Rev. B* (to be published).
- ⁶³W. Gordy and W. J. O. Thomas, *J. Chem. Phys.* **24**, 439 (1956).
- ⁶⁴N. B. Hannay and C. F. Smyth, *J. Am. Chem. Soc.* **68**, 171 (1946).
- ⁶⁵E. Margoliash and A. Schejter, *Adv. Protein Chem.* **21**, 113 (1966).
- ⁶⁶R. G. Shulman, S. H. Glarum, and M. Karplus, *J. Mol. Biol.* **57**, 93 (1971).
- ⁶⁷P. George, J. Beetlestone, and J. S. Griffith, *Rev. Mod. Phys.* **36**, 441 (1964).
- ⁶⁸T. Hoshino and K. Suzuki, *J. Phys. Soc. Jpn.* **48**, 2031 (1980).
- ⁶⁹P. Pecher and G. Toussaint, *Physica* **116B**, 112 (1983).